Surface modified iron-oxide based engineered nanomaterials for hyperthermia therapy of cancer cells

Mehak Dhiman[1]

[1]Affiliation not available

August 30, 2022

Surface modified iron-oxide based engineered nanomaterials for hyperthermia therapy of cancer cells

Mehak[1], Rajkumar P Thummer[2], Lalit M. Pandey[1]*

[1]Bio-interface & Environmental Engineering Lab

Department of Biosciences and Bioengineering,

Indian Institute of Technology Guwahati, Assam, 781039, India

[2]Laboratory for Stem Cell Engineering and Regenerative Medicine

Department of Biosciences and Bioengineering,

Indian Institute of Technology Guwahati, Assam, 781039, India

* Corresponding author: Tel. +91-361-258-3201; Fax +91-361-258-2249

Email addresses: mehak1998@iitg.ac.in, rthu@iitg.ac.in, lalitpandey@iitg.ac.in

Abstract

Magnetic hyperthermia is emerging as a promising alternative to the currently available cancer treatment modalities. Superparamagnetic iron-oxide nanoparticles (SPIONs) are extensively studied functional nanomaterials for biomedical applications, owing to their tunable physio-chemical properties and magnetic properties. Out of various ferrite classes, spinel and inverse-spinel ferrites are widely used but are affected by particle size distribution, particle shape, particle-particle interaction, geometry and crystallinity. Notably, their heating ability makes them suitable candidates for heat-mediated cancer cell ablation or hyperthermia therapy. Exposing SPIONs to an externally applied magnetic field of appropriate frequency and intensity cause them to release heat to ablate cancer cells. Majorly, three heating mechanisms are exhibited by magnetic nanomaterials: Nèel relaxation, Brownian relaxation and hysteresis losses. In SPIONs, Nèel and Brownian relaxations dominate whereas hysteric losses are negligible. These nanomaterials possess high magnetization values capable of generating heat to ablate cancer cells. Furthermore, surface functionalization of these materials imparts the ability to selectively target cancer cells and deliver cargo to the affected area sparing the normal body cells. The surface of nanoparticles can be functionalized with various physical, chemical and biological coatings. Moreover, hyperthermia can be applied in combination with other cancer treatment modalities in order to enhance the efficiency of treatment.

Keywords

Cancer, magnetic hyperthermia, iron-oxide nanoparticles, surface modification, site-specificity, colloidal stability

Introduction

Cancer is one of the fatal, non-communicable diseases with a very high mortality worldwide. Global Cancer Observatory (GLOBOCAN) 2020 estimated 19.3 million new cases with only 48 % survival in the year 2020 (Globocan, 2020). The number of cases is increasing rapidly at the rate of 442.4 per 100,000 men and women per annum and it is estimated that this number would be doubled by the year 2040. Food habits, lifestyle, drugs, exposure to chemicals, high intensity radiations for a long period of time (Blackadar, 2016) and environmental carcinogens (Malik et al., 2021) are a few of the leading causes of cancer. Figure 1 depicts the number of cases reported worldwide in 2020 and mortality due to various cancer types. From the given statistics it can be inferred that the number of cases is the highest for breast cancer whereas, mortality is the highest in case of lung cancer. Concurrently, over the past few years research in the field of cancer treatment has also expanded.

Currently, surgery, radiotherapy, chemotherapy, immunotherapy, hormonal therapy and their combination are being practiced as cancer treatment modalities. Besides, these treatment strategies are associated with side-effects and are not patient-friendly. In this direction, nanotechnology has advanced the medicine and biomedical fields. Nanomedicine is a promising approach for developing effective treatments of different diseases including cancer. Nanoparticles possess excellent physical properties such as small size/high surface-to-volume ratio and unique multifunctional features of stimulus/stimuli-responsiveness. In addition to these properties, magnetic nanoparticles have a heating capacity in response to an externally applied magnetic field (Leonel et al., 2019; Reyes-Ortega et al., 2019).

The effect of heat on biological tissues was known for a long time, which triggered the studies on the hyperthermic effect on tumour cells. Magnetic nanoparticles (MNPs) are excellent candidates for magnetic particle mediated hyperthermia (MPH) or magnetic field hyperthermia (MFH), in which temperature is gradually increased above the normal body temperature to 42-46 °C under the influence of an externally applied alternating magnetic field (AMF). This elevated temperature is considered as the hyperthermia temperature which is safer to the normal tissues to quite a good extent but is able to ablate the tumour tissues (Dahaghin et al., 2021). In addition, with the advent of nanotechnologies, various approaches are being explored so as to apply hyperthermia to deep-seated tumours. Nanomaterials find versatile applications from the field of electronics or environmental remediation (Joshi et al., 2021; Malik et al., 2022) to biomedicine. In recent times, hyperthermia has evolved in which hysteresis and relaxation losses are used to generate heat. The emerging nanotechnologies offer improved and multifunctional nanocarriers to serve the purpose. Multifunctional nanocarriers are highly desired to deliver at the diseased site, treat it and observe the outcome at the same time; generally referred to as nano-theranostics.

In this regard, Iron Oxide Nanoparticles (IONPs) are extensively explored because of their excellent tunable magnetic properties. IONPs are biocompatible, less toxic and physio-chemically stable and thus are being investigated for various biomedical applications. Superparamagnetic iron oxide nanoparticles (SPIONs) possess desired magnetization values and heating ability for hyperthermia applications. Magnetization saturation and Specific Absorption Rate (SAR) values mainly regulate the heating ability of nanomaterials in the applied alternating magnetic field (Tsopoe et al., 2020). The bulk magnetization of magnetite NPs is reported to be 92 emu/g (S. S. Laha et al., 2013) and the highest SAR value reported is 2452 W/g for cubic IONPs (Guardia et al., 2012). Also, taking into consideration the practical constraints on the field parameters in clinical settings,$H \times f < 5 \times 10^9$ A/m.s is generally used for hyperthermia applications (Hergt & Dutz, 2007). Yet, there are few challenges to its practical applications including (i) oxidation of Magnetite (Fe_3O_4) to Hematite (Fe_2O_3) in biological environments, which affects the magnetic properties, (ii) design of superparamagnetic nanomaterials without compromising the saturation magnetization, which can generate hyperthermia temperature, (iii) targeted delivery at the disease site, and (iv) inducing antibacterial properties post-surgery or injury as bacterial infection and biofilm formation can adversely affect the treatment (Nam et al., 2021).

The recent advancements in nanotechnology have enabled the tuning of the physical properties (size, shape,

structure: core-shell/exchange bias (Tsopoe et al., 2020)) and chemical composition (composites, doping with rare earth or transition metals) for broader applications and obtaining improved results. Coating of nanocarriers by organic compounds is desired to ensure their aqueous stability and improve biocompatibility (Jamir et al., 2021). The active biological compounds also offer functional groups which can be advantageous for the functionalization of the nanoparticles. Doping with other metal ions is also reported to improve stability due to the formation of more stable phases (Kowalik et al., 2020). In addition, the nanoparticles can also be conjugated with tumour-specific antibodies or ligand-specific to the respective receptors that are overexpressed in tumour cells to ensure site-specificity (Montazerabadi et al., 2019).

Further, there are several ways in which hyperthermic effects can be enhanced, namely, ultrasounds, radiofrequency, high-frequency currents and microwaves. Among these, the microwave approach is the most promising but is limited to superficial tumours only (Dahaghin et al., 2021). For practical applications, hyperthermia along with other therapeutic approaches such as chemotherapy and radiotherapy are also being exploited. The chemotherapy/radiotherapy sensitizes the tumour cells for further thermal therapy, and thus the synergistic effect of the combined therapies leads to enhanced treatment of cancer (Curcio et al., 2019).

This review summarizes the various iron-based engineered nanomaterials used for hyperthermia applications as an alternative to the currently available cancer treatments. The mechanism of heat generation by IONPs and the various factors affecting their heating ability is discussed. The effect of various dopants on the magnetic properties of IONPs is highlighted. This review also sheds light on the approaches to carrying out surface modification in order to improve the colloidal stability, biocompatibility and target efficacy of MNPs.

Cancer and therapeutic approaches being practiced

Cancer refers to the abnormal and uncontrolled proliferation of normal cells in the body, thereby forming a tumour cell mass. It is said to be malignant or cancerous when it starts to invade other tissues of the body or shows metastasis, while the localized tumour is termed benign or non-cancerous. Hanahan and Weinberg in 2000 described six characteristics of cancer cells, namely uncontrolled growth and differentiation, sustained proliferation, lack of apoptosis, self-sufficiency in growth signals, invasion and angiogenesis (Hanahan & Weinberg). There are hundreds of cancer types arising due to various environmental factors and modern lifestyle habits. Tobacco chewing, exposure to radiation, lack of exercise or physical activities, obesity, infections affecting immunity and pollution are a few of the major causes of cancer (Blackadar, 2016). These factors are responsible for the alterations in genetic makeup leading to mutations, thereby causing cancer. The changes in the principal pathways governing cell proliferation and differentiation are led by multiple genetic events that promote cancer cell growth.

Normal cells regulate their growth and proliferation by acquiring growth signals. Transmembrane receptors help in transmitting these signals into the cells by binding to signalling molecules, such as growth factors, cell to cell interacting/adhesion molecules (CAMs) and extracellular matrix (ECM) components. These signals are crucial for cell proliferation therefore, many oncogenes mimic normal growth signals and lead to uncontrolled tumour cell proliferation. Numerous studies have reported that genetic alterations or mutations such as gain of function in case of oncogenes and loss of function in case of tumour suppressor genes promote cancer cell growth. Oncogenes such as Ras, Myc, BRCA1, etc. are mostly active in cancer cells, whereas tumour suppressor genes, such as p53 and RB1 are mutated to promote tumour progression, thereby acting like a dual-edged sword. Growth factor receptor tyrosine kinase in its cytoplasmic domain is over-expressed in many tumours. The over-expression of receptors makes tumour cells hyper-responsive to the signals to trigger proliferation. For instance, epidermal growth factor receptor (EGFR/*erbB*) is over-expressed in brain, stomach and breast cancers. HER2/*neu* expression is highly upregulated in stomach and breast/mammary carcinomas (Compagni & Christofori, 2000). EGFR is a growth factor receptor tyrosine kinase, generally associated with many types of cancers. It leads to cancer prognosis but also reduces recurrence-free or overall survival rates in the patients. Maurizi *et al.* in 1996 carried out a radio-labelled ligand receptor-based assay and found that elevated levels of EGFR are associated with relapse and death (Maurizi et al., 1996). Besides

this, the unique cell surface markers expressed in cancer cells aid in identifying the different cancer cell types. For example, epithelial-specific antigen receptors, CD44 and CD24, are found to be expressed on the surface of pancreatic cancer cells (Li et al., 2007) and these receptors could be potential targets for cancer therapy.

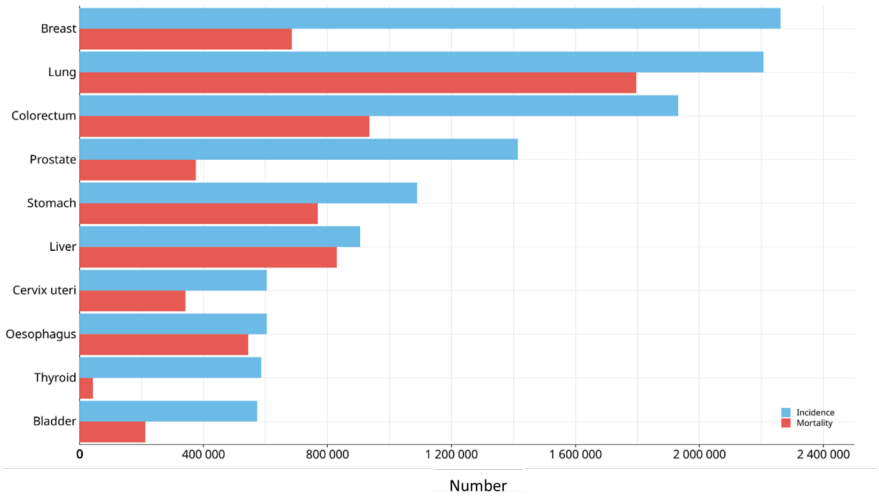

Figure 1: GLOBOCAN statistics for different cancer types depicting the number of cases and mortality. The reported number of cases is almost the same for breast and lung cancer but the mortality is higher in case of lung cancer followed by colorectum and liver cancer. Adapted from ref. (Globocan, 2020).

The current cancer therapies comprise of surgical removal of tumour mass, radiotherapy, chemotherapy, immunotherapy, hormonal therapy and combinatorial therapy. Solid cancers, such as lung, brain, liver, colorectal, stomach and breast cancer, also contribute widely to deaths. Surgical removal of solid cancers is thus considered as a life-saving approach. However, postoperative tumour recurrence is seen in patients. There are evidences to show that surgical tumour resection affects the immune system (J. C. Coffey et al., 2003).

Radiotherapy is generally referred to the usage of X-ray or irradiation therapy to treat malignant tumours. It is one of the main cancer treatments used in about 50% of cancer cases (R. Baskar et al., 2012). It damages cancer cells by the deposition of high-energy radiations in cancerous tissue. Cancer cells are affected by radiations either directly or indirectly. These radiations directly affect the cellular components thus, cause damage to them. The indirect damage to cell genome is caused by the formation of free radicals. It attains its therapeutic efficiency by damaging DNA leading to cancer cell death (R Baskar et al., 2014). It is one of the major cancer therapies available but is associated with side-effects. Thus, the normal body cells are equally prone to fall prey to radiations. In fact, ionizing radiations are potent carcinogens. Secondary malignancies arise after the primary radiotherapy, observed in the case of long-term cancer survivors. A few side effects of ionization radiation include chromosome aberrations, sterility, epilation, cataract and burns depending upon the radiation dosage and site of exposure. For example, an irradiation dose of 3 Gy results in epilation while 6 Gy induces permanent sterility (Aggarwal, 2014).

Chemotherapy is considered as the standard modality, utilizing chemicals/drugs to destroy or inhibit cancer cell growth. Paul Ehrlich, a German chemist first coined the term “chemotherapy” after investigating the use of chemotherapeutic drugs to cure various infectious diseases. On the other hand, patients’ life is adversely affected as they suffer from nausea, anxiety, restlessness, pain, gastrointestinal and sleep disorders. Conventional chemotherapeutic agents used in chemotherapy affect macromolecular (DNA, RNA and protein) synthesis or interfere with their respective functioning. It ultimately leads to cell apoptosis but it may require repeated and high drug dosage (DeVita & Chu, 2008). With repeated drug infusions, the cancer cell may become chemo-resistant by over-expressing reflux pumps and spontaneous mutations, thus the chances

of tumour recurrence increase many folds. To get an adequate response, the use of a combination of drugs is being practiced. While practicing combination chemotherapy, chemotherapeutic drugs with different action mechanisms and non-overlapping cellular toxicities are chosen to escape resistance. For instance, bleomycin, vinblastine and cisplatin are used in combination as a curative regimen for testicular cancers (Elion et al., 1954).

Compared to other standard cancer treatments, immunotherapy has come up with significant improvements in terms of life expectancy and post-treatment life quality. It is a relatively newer approach and is being developed. William B. Coley first attempted to use the immune system against cancer cells in the 19^{th} century and thus is recognized as the "father of immuno-cancer therapy". A cocktail of live, attenuated and inactivated bacteria was prepared, including, *Streptococcus pyogenes* and *Serratia marcescens,*which is known as Coley's toxin (McCarthy, 2006). Upon injecting patients with the toxin, several types of malignancies were reported to be cured. But the unknown mechanism of action and risks associated with it forced oncologists to practice surgery, chemotherapy and radiotherapy. With the improvements and findings in this field, the potential of interleukins (IL), interferons (IF) and chemokines has been discovered to be used for immunotherapy (Dinarello, 2007; Lee & Margolin, 2011). On the other hand, activating the immune response against tumour leads to autoimmunity. The monoclonal antibodies discovered against CTLA-4 and PD-1 (inhibitory immune-checkpoints) have shown antitumour response. Rapidly proliferating cancer cells show high levels of metabolic-reprogramming and a high rate of glycolysis, termed as "Warburg effect", one of the many hallmarks of carcinogenesis (Kareva & Hahnfeldt, 2013). Nutrient scarcity and metabolic waste accumulation takes place in tumour environment as tumour cells limit T-cells to the nutrients essential to activate them and produce higher levels of lactate. CTLA-4 (Gilligan et al., 2000) and PD-1 upon binding to respective ligands inhibit glycolysis by reducing cytokines secretion and exhausting T-cells. Besides glycolysis, amino acids catabolism in the tumour microenvironment is another player in immune function (Patsoukis et al., 2015; Saunders et al., 2005). Tryptophan, L-arginine and glutamine are known to play a role in tumour progression. Thereby, targeting the metabolic pathways of these amino acids may be promising for cancer therapy. The future aspects of immunotherapy may rely on combinatorial therapies. A target directed personalized therapy is highly desirable to prevent tumour recurrence (Esfahani, 2020).

Hormonal therapy is given to patients with advanced or metastatic cancer. It is an effective therapy for prostate cancer and hormone (progesterone and oestrogen) receptor positive breast cancer. It can be given prior to surgery or radiotherapy in order to reduce primary tumour size thereby reducing the recurrence risk. In women with breast cancer, oestrogen suppression is carried out by injecting anti-oestrogen (tamoxifen), oestrogen-receptor antagonist (fulvestrant) and aromatase inhibitor (anastrozole, letrozole, exemestane). Tamoxifen has adverse effects too, such as hot flushes, vaginal discharge, night sweats and high risk of thrombosis. Toxicities associated with aromatase inhibitors include hot flushes, high risk of osteoporosis and arthralgia. In males with prostate cancer, androgen deprivation therapy is given. Luteinizing hormone antagonists are given to reduce serum testosterone to castrate level. Castration may lead to reduced muscle strength, weight gain, sweats, hot flushes, risk of cardiac complications and reduced libido (Abraham & Staffurth, 2016).

Table 1 summarizes the available cancer treatments along with their merits and demerits. Available cancer treatments are useful to some extent in curing cancer, however, are associated with some disadvantages and possess limitations. Neither are they patient-friendly nor economical. Therefore, there is a strong need to develop an alternative cost-effective approach to ensure the elimination of cancer cells without any undesired side effects.

Table 1: Cancer treatments and their merits and demerits

Methods	**Advantages**	**Limitations**
Radiotherapy	Controls the growth of tumour Less time required No effect on daily life	Side effects like tiredness, sickness Damage to normal cells Required special diet High cost

Methods	Advantages	Limitations
Chemotherapy	Shrinks the tumour Reduces the symptoms A cocktail of drugs improves the therapeutic efficiency	Side effects like nausea, fatigue, hair loss May affect patient's health significantly Requires regular visits to doctors, repeated doses required Responsible for rapid mutations and drug resistance among cancer cells
Immunotherapy	Immunomemory generated can prevent the recurrence of cancer Improve the efficiency of other treatment strategies when used in combination Fewer side effects on normal cells	May induce allergic reactions Risk of autoimmune response Takes more time Adaption against the immunotherapy may result in no effect Not generalized, more of a personalized approach Not economical
Surgery	Life-saving approach for solid tumours	Highly invasive Highly painful Chances of tumour relapse are very high
Hormonal therapy	Given to the patients with advanced or metastatic cancer Effective for prostate and breast cancers	Hot flushes, vaginal discharge, night sweats and high risk of thrombosis, in case of females Reduced muscle strength, weight gain, sweats, hot flushes, risk of cardiac complications and reduced libido, in case of males

Hyperthermia: A novel approach

Hyperthermia refers to an increase in temperature to 42-46 °C, which has the potential to induce cancer cell ablation. Extensive research is being carried out in this field. Many randomized clinical trials have demonstrated that the effectiveness of other treatments, such as radiation therapy and chemotherapy, is enhanced when used in combination with hyperthermia (Hynynen & Lulu, 1990). However, its full potential as an independent, therapeutically relevant treatment strategy is yet to be realized in medicine. Moreover, it has not gained much attention to date due to its inability to heat malignant cells efficiently and locally. Conventional hyperthermia also possesses side effects as both malignant as well as non-malignant cells are heat labile. This issue can be avoided by administering magnetic nanoparticles targeting specifically cancer cells which are capable of accumulating in the affected/cancerous tissues. Tumorigenic tissue can then be subjected to hyperthermia temperature on the application of AMF in order to ablate it. This focused technique allows for localized heating of cancer cells while avoiding damage to adjacent normal tissues, potentially increasing its efficacy and safety (Giustini et al., 2010).

There is a wide range of mechanisms through which hyperthermia can cause cellular damage as there is a significant difference in the heat lability of cancerous and normal cells of the body. Cancer cells are more sensitive to heat (Campbell, 2007). *In-vitro* experiments have shown that temperature and hyperthermia duration affect cell viability. In a study done by Haghniaz *et al.* , the therapeutic potential of dextran-coated MNPs was analyzed for hyperthermia application. The prepared MNPs were subjected to different temperatures of 43, 45 and 47 °C for 0-24 h of time intervals. At hyperthermia temperature of 43 °C, cells became thermotolerant whereas, in the case of hyperthermia treatment for 24 h at 45 °C and 47 °C tremendous cell death was observed because of the elevated levels of Heat Shock Proteins (HSPs) responsible for inducing apoptosis (Haghniaz et al., 2015). The sensitivity of cells towards hyperthermia requires tissue temperature to

rise evenly and distribute MNPs homogenously in cancer cells. Thus, sufficient exposure of malignant cells to the hyperthermia temperature for an appropriate time period can kill them (Oei et al., 2015). With regard to the killing mechanisms, protein denaturation ensuing downstream pathways activation or deactivation could be one of them. Proteins start to denature at 40 °C and at higher temperatures a large protein proportion is likely to be denatured (Dickson & Oswald, 1976). As the hyperthermia temperature range is from 42-46°C, protein denaturation does not occur to a great extent. However, a few of the denatured proteins aggregate with the native ones. Thus, as a result of protein denaturation and aggregation, DNA repair, protein synthesis and cell cycle progression pathways are severely affected. Also, heat induces alterations in membrane proteins and damages the plasma membrane. The elevated tissue temperature reoxygenates the tumour microenvironment by increasing the blood supply to the tumour tissue. As shown in figure 2, magnetic hyperthermia treatment (MHT) leads to immunomodulation by triggering an immune response against tumour. Heat shock proteins (HSPs) play a crucial role in antigen recognition by dendritic cells. HSP-bound antigens are presented to the major histocompatibility complex I (MHC-I) molecules, which thus leads to T-cell activation or lymphocyte trafficking. HSP 60 protein is found to be involved in activating T-cells thereby, allowing IFN-γ secretion. Also, MHT is found to upregulate HSP 70 expression which provokes the immune system against tumour prognosis (Mahmood et al., 2018).

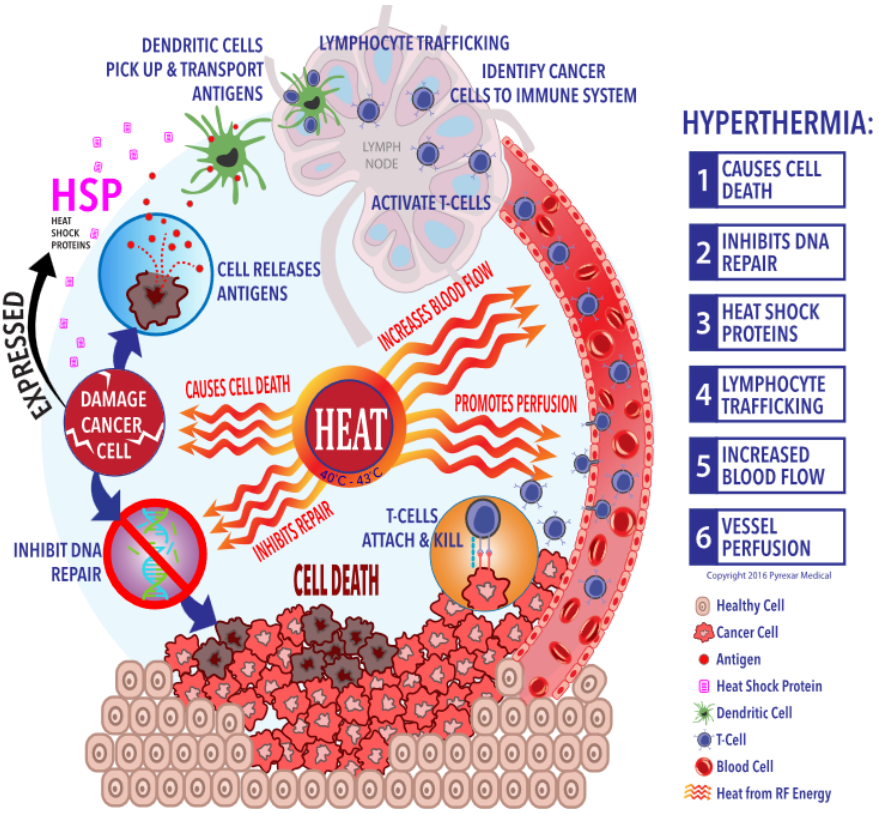

Figure 2: Immunomodulation by magnetic hyperthermia treatment. Heat generated by NPs inhibits or denatures DNA repair enzymes, reoxygenates tumour microenvironment by increasing vessel perfusion and leads to over-expression of HSPs which are then presented to immune cells as antigenic entities thereby leading to lymphocytes trafficking at tumour site. Adapted from ref. (Pyrexar Medical, 2015).

In-vivo investigations have revealed some unique mechanisms via which hyperthermia affects cancerous cells. Tumours possess fenestrated vasculature which is responsible for their acidic and hypoxic environment. Cancerous cells thus fall susceptible to hyperthermic conditions. Poor vasculature and increased temperature

pave the way for easier delivery of chemotherapeutic drugs and higher oxygen diffusion, sensitizing cells to chemotherapy and radiotherapy, respectively (Muz et al., 2015). Thus, when given in combination with other therapies in use, hyperthermia can provide clinicians with better treatment outcomes.

There are various ways in which hyperthermia can be given and is broadly categorized (figure 3) as conventional and localized approaches. The conventional approach includes whole-body and regional hyperthermia. In the case of whole-body hyperthermia, hot blankets and thermal chambers are used to raise body temperature whereas, in regional hyperthermia perfusions with hot liquids are given to the patient. The localized approach is divided into external and nanoparticle-based hyperthermia. In the case of external hyperthermia, a focused radiation beam is given to elevate tissue temperature but is beneficial for superficial tumours only. Nanoparticle-based hyperthermia involves the use of MNPs injected into the patient to generate heat locally.

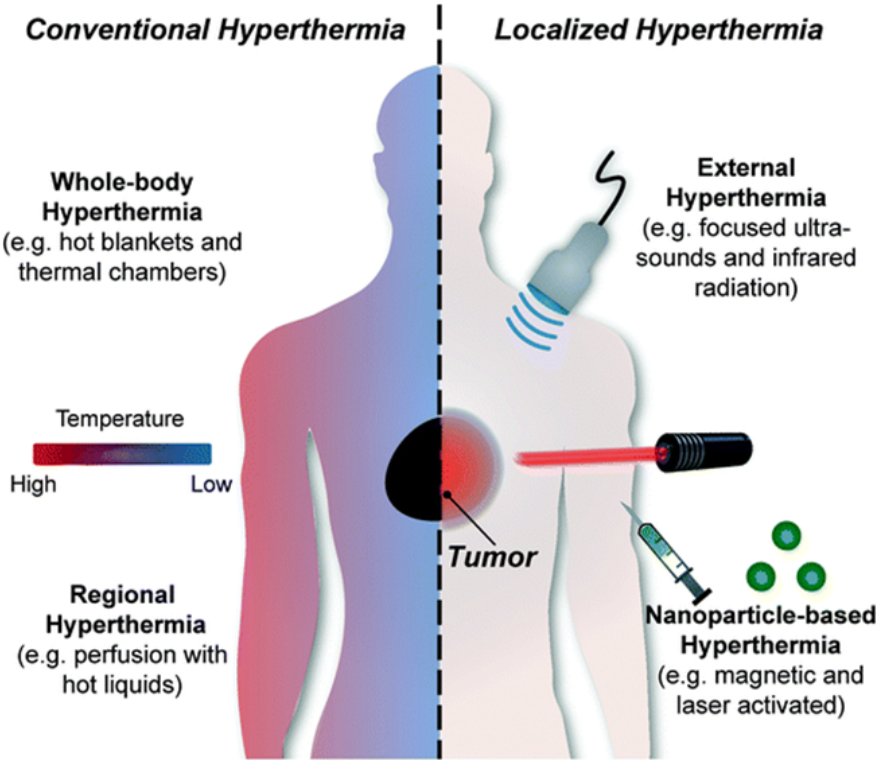

Figure 3: Broad classification of hyperthermia as conventional and localized approach depending upon the heat source used to ablate cancerous tissue. Adapted with permission from ref. (Fernandes et al., 2020).

Magnetic Hyperthermia

Malignant and non-malignant tissues show similar responses to hyperthermia and/or combinatorial therapy (Dickson & Oswald, 1976). This acts as a barrier to its clinical application. Therefore, magnetic hyperthermia comes with a concept that shows promise in overcoming clinical barriers. SPIONs due to their tunable physicochemical properties and high surface area to volume ratio are desirable candidates for magnetic hyperthermia. In 1957 Gilchrist et al., for the first time came up with the concept of using magnetic iron oxide nanoparticles (MIONs) in cancer treatment. They injected 20-100 nm sized MIONs into the lymphatic channels to ablate residual malignant cells on the application of AMF (Gilchrist et al., 1957). Jordan et al. in 1993, directly injected MNPs into the tumour and showed that this approach leads to selective heating of tumour mass (Jordan et al., 1993).

Soon after the realization of the potential of magnetic hyperthermia, a surge could be seen in industries to design and develop a hyperthermia setup. MagForce AG, a Germany-based company, founded in 1997, produces devices for magnetic hyperthermia applications. It has designed NanoTherm® (aminosilanized-ferrofluids), NanoPlan® (software for temperature simulations), NanoActivator® (AMF applicator). The UK-based company nanoTherics (founded in 2007), designs biomedical instruments. MagneTherm® is one of the products designed by this company for MNPs heating applications, including *in-vivo* ,*in-vitro* , calorimetric and drug release.

Specific Absorption Rate (SAR) or Internal Loss Power (ILP) value of MNPs is used to define their heating ability or efficiency to be used as hyperthermia agents. Guardia *et al.* reported the highest SAR value of 2452 W/g for 19 nm Iron Oxide Nanocrystals (IONCs) at a concentration of 1 mg/mL (Guardia et al., 2012). Similarly, the highest SAR value (1588.83 W/g) has been reported by Peng *et al* for 14 nm manganese ferrite nanoparticles (MFNPs) even at a very low concentration of 0.1 mg/mL. Though a higher SAR value is beneficial to minimize the dose of MNPs formulation and thereby reducing its toxicity, it possesses some constraints (wPeng et al., 2012). MNPs even with higher SAR values can possess toxicity or biocompatibility issues (Malhotra et al., 2020). Having so many reports on the use of MNPs for hyperthermia application, challenges like crystalline size (within range of critical particle size), improved magnetization saturation (M_s), reduced cytotoxicity or better biocompatibility, and colloidal stability, are common challenges that still need to be addressed. In this regard, doping of the magnetic materials with other materials can be employed to have the desired magnetic heating outcome. Also, in order to make these nanomaterials colloidally stable, biocompatible and site-directed, surface functionalization or coating can be carried out. Therefore, it is of great attention to develop novel MNPs that (1) generate heat which is well-distributed in tumour cells to eliminate them, (2) require minimal dosage and (3) must be site-directed.

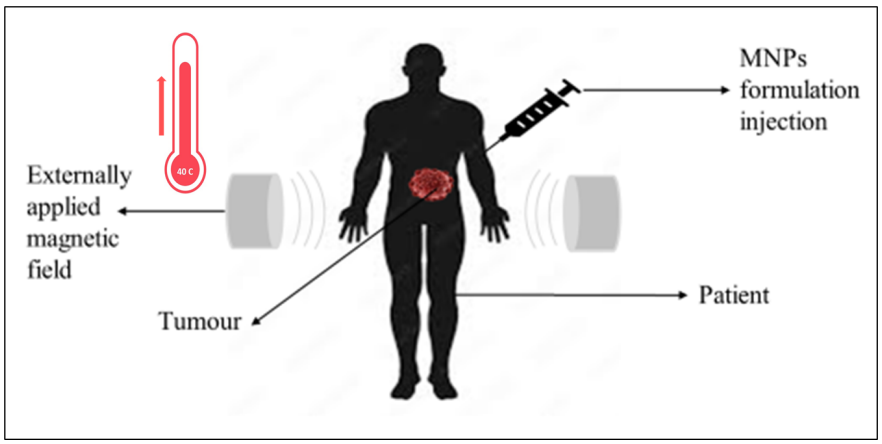

Figure 4: Schematic of MFH showing nanoformulation being injected to the patient and application of AMF to generate heat for hyperthermia treatment.

Mechanism of heat generation by MNPs

The magnetic materials possess magnetic moments or dipoles in addition to which they exhibit some characteristics on exposure to AMF: saturation magnetization (M_s), remanence/remanent magnetization (M_r), coercivity/coercive field (H_c) (Dennis & Ivkov, 2013). When exposed to an external magnetic field, SPIONs magnetic domains align with the direction of AMF and the saturation magnetization (M_s) is achieved with the alignment of all the magnetic domains. Removal of the applied field de-aligns the magnetic domains

but does not lose their magnetization completely. The remaining magnetism is referred to as*remanent* magnetization or remanence (M_r). Brollo*et al.* in 2016 reported that M_r is responsible for the aggregation of particles (Brollo et al., 2016). The magnetic field applied to remove remanence is called a coercive field or coercivity (H_c). SPIONs do not possess coercivity and remanence magnetization, as shown in figure 5. SPIONs do not agglomerate much due to the magnetic interactions which makes them suitable candidates for biomedical applications.

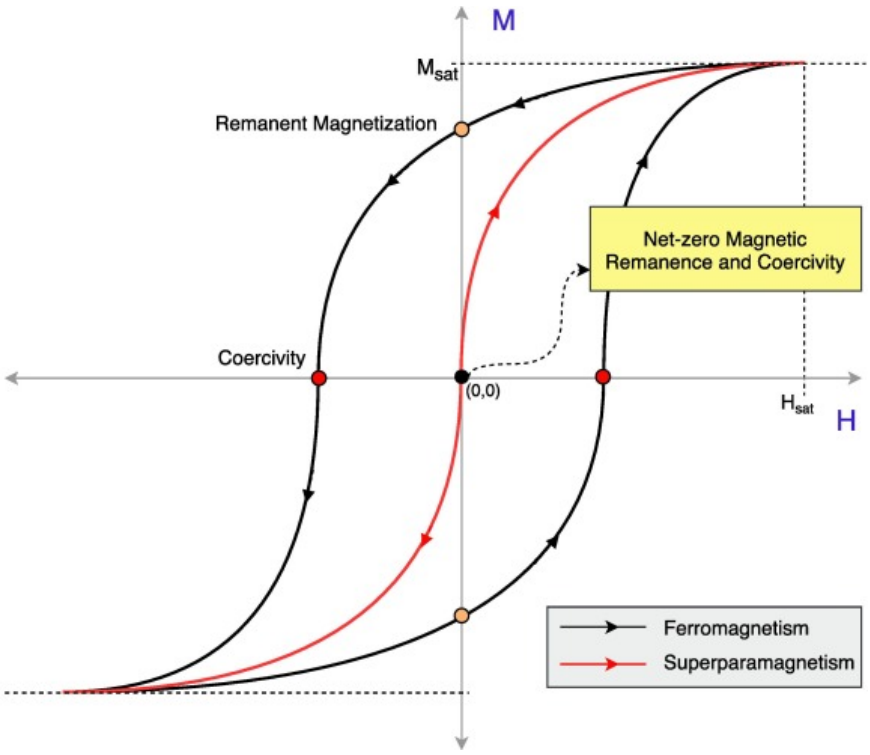

Figure 5: M-H curve for the superparamagnetic material is shown in red and for ferromagnetic material in black. For a superparamagnetic material, $M_r$and H_C are negligible. Adapted from ref. (Sezer et al., 2021).

The applied alternating magnetic field is responsible for heating the MNPs by one of the mentioned mechanisms: Brownian relaxation, Nèel relaxation, eddy currents and hysteresis loss. Magnetic materials possess dipoles having both, magnitude and direction. AMF application forces the dipoles to align with it. The magnitude or strength of AMF and properties of the material affect the extent of alignment. The direction of the magnetic moment of a material changes upon a change in polarity of AMF. Body tissues are electrically conducting so, upon their interaction with AMF, eddy currents are induced. As a result of which, Joule heat is deposited in the tissues which is in accordance with the Faraday's Law of induction. Eddy currents thus can lead to excessive tissue heating and are undesirable. The non-specific tissue heating due to eddy currents can be controlled by tuning AMF amplitude (Attaluri et al., 2020). Hysteresis is an inherent property of a magnetic material in which its saturation vector traces a loop rather than retracing a single path on exposure to an oscillating magnetic field. The hysteresis mechanism varies for magnetic materials that possess single and multiple domains. When material consisting of multiple domains is given an oscillating magnetic field, hysteresis occurs from the reorganization of domains. While in materials possessing a single domain, magnetization reversal may arise from the coherent rotation of dipoles. The reversal does not take place if the anisotropy of a sample is higher than the amplitude and frequency of AMF leading to hysteresis. Hysteresis losses lead to the heating of the magnetic material (Banerjee et al., 2010). The higher the anisotropy of a magnetic material, the higher is the hysteric loss, leading to increased heat generation or Specific Loss Power

(SLP). Higher SLP values are observed for nanomaterials as compared to their respective bulk material (Hu & Du, 2009; Krycka et al., 2010). Heat generation by hysteresis loss is in accordance with the first law of thermodynamics; $U = dQ + dW$ (Dennis & Ivkov, 2013), where, U is the change in energy, $\mathrm{d}Q$ represents heat and $\mathrm{d}W$ is the work done. The work required to magnetize a magnetic material is given by the following equation (Equation 1),

$$dW = \mathrm{H} \bullet dM \quad (1)$$

where, H is strength of AMF and M represents magnetization. M and H are related to the magnetic flux density (B): $B = \mu_0(H+M)$ where, $\mu_0$is the vacuum magnetic permeability.

As mentioned earlier, the magnetization saturation vector does not follow the same path but traces a loop. Hence, net work is done which is then converted into heat, given by the following equation (Equation 2),

$$W_{\mathrm{heat}} = \oint \mathrm{H} \bullet dM \quad (2)$$

The area under the hysteresis loop is therefore given by equation 2. There are two types of hysteresis loops, namely the major and the minor loop. The major loop begins at $\mathrm{M_s}$ when all the dipoles align parallel to that of AMF, going to negative saturation and back. In a minor loop, the maximum applied field is less than the field required to achieve $\mathrm{M_s}$ or is unable to saturate the magnetic system. The maximum heat ($\mathrm{H_{max}}$) is generated by magnetic materials upon tracing the major hysteresis loop. However, in the case of hyperthermia, heat is generated from the minor loop as there are limits on field parameters from the perspective of patient's safety and economical feasibility. Thus, practical constraints arise in the design of the instrument. Biological constraints, such as material choice, particle size and field strength are also there in the practical application of hyperthermia (Atkinson et al., 1984). Different research groups have given different values for the field parameters as given in table 2.

Rosensweig for the first time gave the concept of heat approximation generated by magnetic particles in the presence of AMF (Rosensweig, 2002). A linear response of magnetization to AMF is assumed giving the following equation (Equation 3),

$$\chi = \chi^{'} - \imath\chi^{"} \quad (3)$$

where, χ called susceptibility $\left(= \frac{M}{H}\right)$, for a given amplitude of AMF is considered constant. This approach is referred to as the Linear Response Theory (LRT). The power dissipation is given by,

$$P = \mu_0 f \oint \mathrm{H} \bullet dM \quad = \mu_0 \pi \chi^{"} f H^2 \quad (4)$$

Brownian relaxation time, τ_{B} is the physical rotation of the MNPs along with the magnetic moment given by equation 5, whereas, Nèel relaxation time, τ_{N} is the internal rotation of magnetic moments with hysteresis given by equation 6 (Maldonado-Camargo*et al.* 2016) (Maldonado-Camargo et al., 2017),

$$\tau_B = \frac{3\eta V_H}{k_B T} \quad (5)$$

$$\tau_N = \tau_A \left(\frac{\sqrt{\pi}}{2}\right) \left(\sqrt{\frac{k_B T}{K V_M}}\right) e^{k V_M / k_B T} \quad (6)$$

where, K is anisotropy constant, η is fluid viscosity, V_H represents hydrodynamic volume of NPs, K_{b} refers to the Boltzmann's constant and T denotes the temperature. The amplitude or frequency does not affect Brownian relaxation. The effective relaxation time constant (τ) is related to the Brownian relaxation time and Nèel relaxation time by the following expression (equation 7) (W. T. Coffey & Kalmykov, 2012),

$$\frac{1}{\tau} = \frac{1}{\tau_B} + \frac{1}{\tau_N} \quad (7)$$

Power dissipation expression can also be depicted by the following expression (equation 8) in the modified LRT (Rantschler et al., 2007),

$$P = \mu_0 \pi \chi_0 f {H_0}^2 \left(\frac{2\pi f \tau}{1+[2\pi f \tau]^2}\right) \quad (8)$$

where, μ_o is the free space permeability, $\chi_0$is equilibrium susceptibility, H_0 is amplitude and f is the frequency of applied AMF. The expression shows the relation between heat generation and frequency, relaxation time and parameters of AMF.

The heating ability/efficiency of MNPs is generally expressed in terms of SAR value. SAR value is the ratio of power dissipated per unit mass of MNPs (equation 9) (Cristina & Samia, 2016),

$$SAR = \frac{P}{m_{\mathrm{MNP}}} \quad (9)$$

where P is power dissipated and m_{MNP} is a unit mass of magnetic nanoparticles. Another way of expressing SAR value is,

$$SAR = \frac{m_s}{m_n} C_p \frac{T}{t} \quad (10)$$

where, C_p is specific heat of the solvent, m_s denotes mass of solvent, m_n is mass of MNPs and $\frac{T}{t}$ is initial slope of the heating curve.

MNPs heating ability can also be expressed in terms of Specific Loss Power (SLP), also called Intrinsic Loss Power (ILP). The rationale behind introducing SLP/ILP was to compare the heating efficiency of MNPs at different values of amplitude and frequency of AMF (Kallumadil et al., 2009).

$$SLP = \frac{\mathrm{SAR}}{fH^2} \quad (11)$$

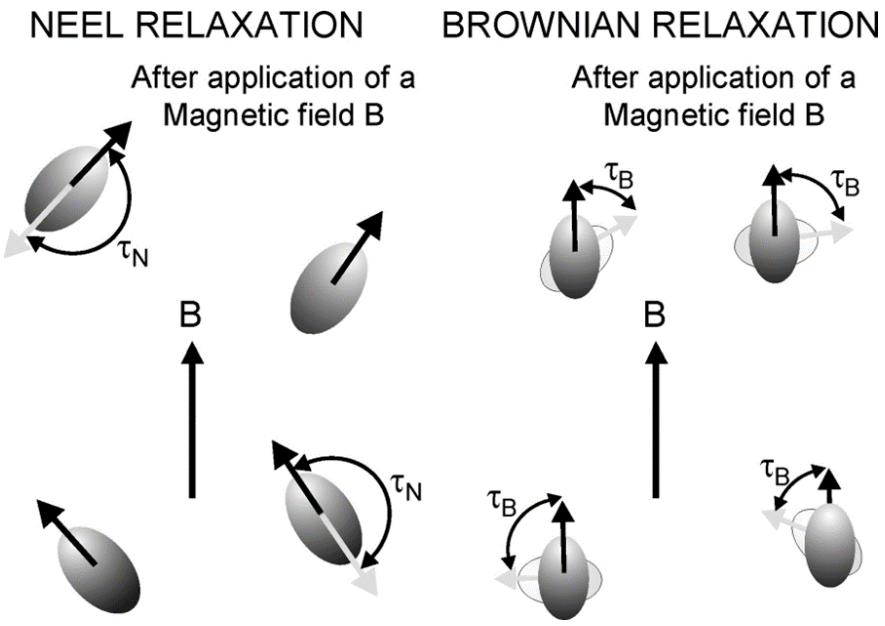

Figure 6: The rotation of particles after the application of AMF causing Brownian relaxation and the rotation of dipoles in accordance with the applied field leading to Nèel relaxation. Adapted with permission from ref. (Laurent et al., 2008).

Factors affecting the heating ability of MNPs

IONPs are being developed for efficient magnetic hyperthermia performance. Exposing IONPs to AMF of appropriate frequency and intensity cause them to release heat to ablate cancer cells. The available nanomaterials for MFH must be improved in order to access deep-seated tumours, reduce dosage, limit field parameters to biologically specified levels, increase SAR value and subsequently increase heating output.

Literature shows spherical IONPs with a size of about 20 nm are suitable for MFH application (Gazeau et al., 2008). Whereas, the studies carried out with field conditions of$H \times f < 5 \times 10^9$ A/m.s suggest spherical IONPs with 14 nm diameter to be optimal for MFH (Gazeau et al., 2008; Kolosnjaj-Tabi et al., 2014). This provides a wide optimal range of 12-20 nm for IONPs. IONPs magnetic properties are strongly influenced by the SAR value which further depends on the field parameters (frequency and strength/field intensity), size distribution, magnetization and magnetic anisotropy of the MNPs and particle-particle interaction.

Size and shape: The prime mechanisms governing thermal losses include hysteresis loss, Néel and Brownian relaxation. The size of NPs dictates which one of these mechanisms will dominate. Hysteresis losses are dominated in NPs [?] 100 nm, but are very large for practical biomedical or clinical applications (Issa et al., 2013). For magnetite, the critical size is 15 nm, below which superparamagnetism is observed i.e., hysteresis losses become negligible and Neel and Brownian relaxation govern the heating mechanism in IONPs (Mohapatra et al., 2018a). Size and shape of nanoparticles greatly affect their magnetic properties and hence the magnetization. A high value of magnetization along with high induction heating loss power is exhibited by small-sized particles but ¡ 5 nm sized particles lead to surface-spin disorders lowering the magnetization value. Also, the critical size for SPIONs is 20 nm beyond which their superparamagnetic character (Nèel and Brownian relaxation) disappears. Taking into consideration these constraints, the optimal particle diameter should range between 5-20 nm (Oh et al., 2016). In a study by Muller *et al* ., the effect of changing particle size on SAR value was investigated. MNPs of sizes ranging 10-20 nm were prepared by the co-precipitation method. It was found that the smaller NPs of size 10-12 nm show superparamagnetic behavior whereas, larger NPs of size 15-20 nm showed ferrimagnetic behavior. The NPs with 12-15 nm showed higher SAR values (Müller et al., 2013). Gonzalez-Fernandez *et al.* synthesized IONPs with sizes ranging from 5-110 nm. Under the field parameters of 13 kA/m and 260 kHz, 30 nm sized IONPs showed maximum heating efficiency. With the increasing size, the SAR value was found to decrease and at particle diameter of 110 nm with multiple-domain, SAR value diminished (Gonzalez-Fernandez et al., 2009). Presa *et al.* (De la Presa et al., 2012) made an attempt to study the effect of size on the heating efficiency of IONPs. NPs in the size range of 6-14 nm were synthesized. All the samples were analyzed for their hyperthermia performance keeping concentration constant (50 µg/mL) under constant field parameters ($H\ _0f < 5 \times 10^9$A/m.s). From this study, a nearly cubic-dependence of SAR value on NPs radius was observed as:

$$SAR \propto \left(\frac{d}{2}\right)^3$$

Besides the size, the shape of the nanoparticles also influences their magnetic properties. Moreover, there is a restriction on modifying the size of IONPs as their superparamagnetic character vanishes beyond a certain limit. To circumvent this problem, another possibility is modifying their shape/composition. The shape of NPs can be manipulated by controlling the growth rate. Gonzalez-Fernandez *et al.* have shown that the addition of ethanol during NP fabrication yields cube-shaped NPs by slowing down the growth rate (Gonzalez-Fernandez et al., 2009). Guardia *et al.* also showed that the cube-shaped iron-oxide nanocrystals (IONCs) of 19 nm diameter possess the highest SAR value of 2452 W/g. J. K among all the various sized synthesized IONCs (Guardia et al., 2012). Tabi *et al.* investigated the efficacy of PEGylated iron-oxide nanocubes with a 19 nm of diameter. These nanocubes with a low dose of 700 μg_{Fe} could de-structure the tumour microenvironment (Kolosnjaj-Tabi et al., 2014). Mohapatra *et al.* synthesized ferrite nanoparticles with different shapes, namely spheres and rods. Both the nanoparticles displayed superparamagnetism with high M_s values. 50 nm sized rod-shaped MNPs possessed M_s value of 58 emu/g and spherical-shaped 16 nm MNPs had M_s value of 83 emu/g (Mohapatra et al., 2018b). Octopod-shaped NPs have also been reported to possess high SAR values. Nemati *et al.* reported 70% increase in the SAR value from 140 to 240 W/g after tuning the shape and size of IONPs (Nemati et al., 2016).

There is ample experimental data available for the effect of size and shape on the heating abilities of NPs in terms of their SAR value. However, there is no established mathematical relation between SAR value and size and/or shape of the NPs. Likewise, for cobalt-ferrites the optimal size is estimated to be 6 nm (Caizer,

2021). Moreover, it is based on theoretical calculations only and experimental data is needed to support the statement.

Field parameters: As described in equation 4 above, the power dissipation of MNPs is directly proportional to the square of the AMF amplitude (H). Hence, the SAR value is affected by the field parameters as well. SAR value increases with increasing field strength. However, there are constraints on field strength in clinical settings, as high frequency and large amplitude magnetic field produces local heating by inducing eddy currents. Brezovich *et al.* found$H \times f < 4.85 \times 10^8$ A/m.s to be safer for humans (Atkinson et al., 1984). Hergt *et al.* recommended the *Hf*limit to be $\leq 5 \times 10^9$ A/m.s (Hergt & Dutz, 2007) taking into consideration the patient's safety against the excessive heating caused by eddy currents. As summarized in table 1 below, different research groups have put forward different values for the field parameters used for hyperthermia application. But this range is further reduced due to technical constraints. Frequencies in the range of 100-150 kHz and amplitude ranging from 10-30 kA/m are generally used for biological settings.

Table 2: Various field parameters used for magnetic hyperthermia applications

Research groups	**H×f** (A/m.s)	**References**
Brezovich *et al.*, 1984	[?]4.85×10^8	(Atkinson et al., 1984)
Hergt *et al.*, 2007	[?]5×10^9	(Hergt & Dutz, 2007)
Jordan *et al.,* 2008	[?]1.8×10^9	(Thiesen & Jordan, 2008)
Mamiya *et al.,* 2013	[?]2×10^9	(Mamiya, 2013)

Anisotropy and particle-particle interactions: In order to improve the heating ability of MNPs, tuning their magnetic anisotropy is also an option. To achieve this, research in the direction of core-shell MNPs is attracting attention. Modulating the surface anisotropy of MNPs also helps improve their heating ability. The exchange bias coupling taking place between the core-shell is responsible for tuning the magnetic properties of the MNPs. In the bi-magnetic nanomaterial consisting of a core and a shell composed of an antiferromagnetic and ferri/ferro-magnetic material, the coupling between the uncompensated spins of antiferromagnetic material with the spins of ferri/ferro-magnetic material at their magnetic interface leads to the shift in hysteresis curve (Barrera et al., 2018; Cotin et al., 2019; Lavorato et al., 2018; Simeonidis et al., 2020). The investigations into heating ability of the MNPs due to exchange bias have been carried out and also the normal and inverted core-shell nanomaterials for hyperthermia applications are being exploited. Tsopoe *et al.*carried out a comparative study between the exchange bias effect of normal core-shell and inverted core-shell nanomaterials. They synthesized core-shell nanostructures consisting of antiferromagnetic (NiO) and ferrimagnetic (Fe_3O_4). An inverted core-shell nanostructure consisting of NiO core and Fe_3O_4 shell and a normal core-shell nanostructure with Fe_3O_4 core and NiO shell were prepared. Also, their influence on the heating efficiency of MNPs was studied. The extensive study of their magnetic properties revealed that despite having lower M_s values than the bare ferrites both the nanostructures (normal core-shell and inverted core-shell) possess high SAR as compared to the single-phase consisting ferrites which can be attributed to the exchange bias coupling at the core-shell interface. Moreover, inverted core-shell nanostructures showed a higher SAR value of 278 W/g when compared to that of normal core-shell nanostructures (232 W/g) owing to their higher surface anisotropy due to more exchange bias coupling. The greater exchange bias coupling in case of inverted core-shell nanostructures is because of the uncompensated spins of dipoles at the antiferromagnetic interface. The average particle size for bare ferrite NPs was found to be 40.76 ± 3 nm which reduced to 36.44 +- 2 nm for inverted core-shell nanostructures and 31.75 +- 3 nm for normal core-shell nanostructures. According to the authors, the diffusion of layers of constituents during core-shell formation is responsible for the reduction in the size. Furthermore, both the core-shell nanostructures were found to reach hyperthermia temperature in about 10 minutes and showed a good cytocompatibility with ¿ 75 % cell viability upto a concentration of 1 mg/mL (Tsopoe et al., 2020). Gupta *et al.* prepared magnetite-Zn-oxide core-shell nanoparticles. ZnO-MNPs find wide applications in cancer treatment, photosensitizer, biosensing,

drug delivery and are well-known for antibacterial properties. Therefore, the authors devoted efforts to develop the nanoplatform bearing Fe_3O_4core and ZnO shell NPs via a two-step chemical synthesis approach. Fe_3O_4 synthesized by the hydrothermal method was then deposited with a ZnO shell. They were found to exhibit superparamagnetic behavior and excellent heating efficiency. The SAR value of bare NPs was found to be 92 W/g and that of core-shell NPs was 80 W/g and M_s value of 35 emu/g and 32 emu/g, respectively with negligible remanence and coercivity. Also, the ILP value was calculated and found to be 0.58 for bare and 0.49 nHm^2/Kg for core-shell NPs. This clearly indicates that the ZnO coating did not affect the SAR, M_s and ILP values much and they were found to be within the range of commercially available ferrofluids. The prepared core-shell NPs reduced HeLa cell viability to 50% on 5 minutes exposure to AMF which can be attributed to the Reactive Oxygen Species (ROS) production by ZnO. They also studied the photoluminescence properties of the prepared NPs at room temperature. The emission of Fe_3O_4 -ZnO core-shell NPs was observed in the visible range, promising for bio-imaging. The prepared multifunctional NPs have the potential to be used in bioimaging and hyperthermia (Gupta et al., 2021).

Iron-oxide based nanomaterials used for magnetic hyperthermia

When subjected to AMF, MNPs are capable of generating heat via the magnetic relaxation mechanism, as discussed above. Many native magnetic nanoparticles, such as Fe, Ni and Co, as well as their oxides, have been studied for their possible use in hyperthermia. Owing to their remarkable size-dependent magnetic characteristics, simplicity of functionalization, biocompatibility, ease of excretion and proven chemistry, nanoferrites are being exploited for biomedical applications in magnetic hyperthermia treatment. Among iron oxides; magnetite (Fe_3O_4) and maghemite (γ-Fe_2O_3) are suitable candidates for biomedical applications. However, γ-Fe_2O_3 is prone to oxidation, whereas Fe_3O_4 is relatively stable (Múzquiz-Ramos et al., 2015). Ferrites can be classified based upon their crystal structure and according to a magnetic field. Depending upon the crystal structure ferrites can be classified as spinel ferrites (normal, inverse and random) bearing the general formula AB_2O_4, hexagonal ($AB_{12}O_9$), garnet ($M_3Fe_5O_{12}$ where, M is any metal) and ortho ferrites ($RFeO_3$ where, R denotes rare-earth metals). On the other hand, according to their susceptibility towards magnetic field, ferrites are classified as soft and hard ferrites. Out of various ferrite classes, spinel and inverse-spinel ferrites are used extensively and are affected by geometry and crystallinity (Manohar, Chintagumpala, et al., 2021).

Fe_3O_4 (magnetite) has an inverse-spinel structure with the formula ($B(AB)O_4$), in which Fe^{3+} occupies the tetrahedral (A) sites and Fe^{2+}/Fe^{3+} are placed alternatively at octahedral (B) sites (Gubin, 2009). Superexchange interactions between Fe^{2+}/Fe^{3+} ions and oxygen ions are responsible for magnetism in Fe_3O_4. Single-domain Fe_3O_4 shows interesting magnetic properties. Fe_3O_4 NPs of lesser than 20 nm size (critical diameter) exhibit zero remanence and coercivity, hence the superparamagnetic behavior. Bulk magnetite (Fe_3O_4) is reported to show a very high magnetization saturation value (M_s) of 92 emu/g (S. S. Laha et al., 2013). However, M_s is found to decrease with an increase in surface-to-volume ratio due to the surface spin-canting (Gubin, 2009). The first study to report the highest SAR value for IONPs was carried out by Guardia *et al.* where water-soluble cube-shaped iron-oxide nanocrystals (IONCs) were synthesized via one-pot (co-precipitation) synthesis. Different sized IONCs were synthesized in the size range of 13-40 nm. For all the IONCs, it was observed that the SAR value increases linearly with increasing field parameter i.e., frequency as can be seen from Figure 7A. On the other hand, square dependence of SAR was observed upon fixing the frequency against AMF amplitude (Figure 7C, 7D). SAR value dependence of different sized-NPs (12, 19, 25 nm) on *Hf* factor at a frequency of 320 kHz and SAR value dependence of 19 nm NPs on *Hf* factor at varying frequencies of 320, 520 and 700 kHz was also analyzed as can be seen from Figure 8. Among all the synthesized samples, IONCs having a diameter of about 19 nm showed a significantly higher SAR value of 2452 W/g with a field strength of 520 kHz and 29 kA/m. This was the highest SAR value reported for IONCs to date. Also, an in-vitro study on KB tumour cells was carried out with 19 nm IONCs resulted in 50% of cell mortality in 1 h at the hyperthermia temperature of 43 °C (Guardia et al., 2012).

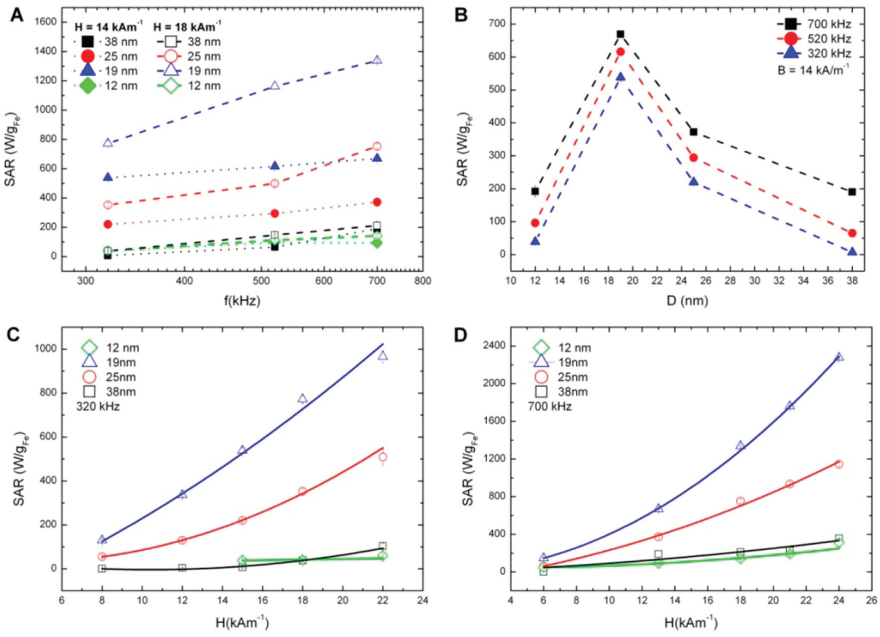

Figure 7: SAR value (W/g) dependence on (A) frequency and amplitude of 14 kA/m (solid symbols) and 18 kA/m (void symbols) for various sized IONCs, (B) as a function of size for varied frequencies 320, 520 and 700 kHz, (C) AMF amplitude with a frequency of 320 kHz for different sized-IONCs, (D) AMF amplitude with a frequency of 700 kHz for different sized-IONCs. Adapted from ref. (Guardia et al., 2012).

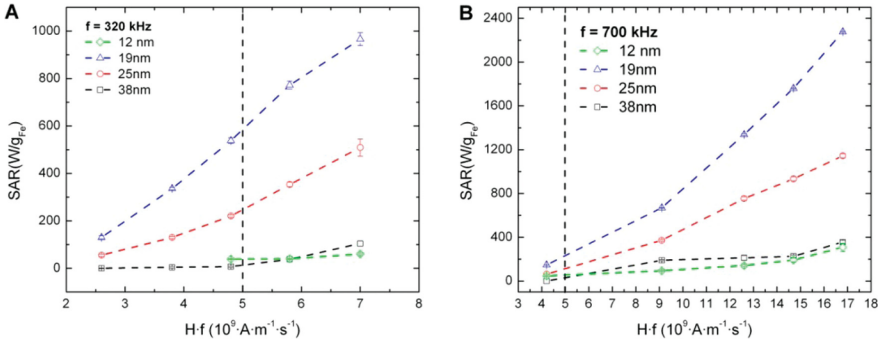

Figure 8: (A) SAR value dependence of different sized-NPs on *Hf* factor at a frequency of 320 kHz, (B) SAR value dependence of 19 nm NPs on*Hf* factor at varying frequencies of 320 kHz, 520 kHz and 700 kHz. Adapted from ref. (Guardia et al., 2012).

IONPs possess a high T_c value because of which they are not appropriate for hyperthermia application. This is mainly because of the amount of heat that may be delivered to the cells is limited. Thus, doping another material into the iron oxide is considered to be the simplest and straightforward approach to improve its magnetic characteristics. Doping materials such as Co, Zn, Ni and Mg can be employed to have the desired magnetic heating. In a study by Sonia*et al.* , the role of substituting high anisotropy Co in Fe_3O_4 on its magnetic and structural properties was investigated. Oleic acid was used as a surfactant in the co-precipitation synthesis of cobalt (Co^{2+}) substituted Fe_3O_4. X-ray diffraction (XRD) and Rietveld refinement confirmed inverse-spinel structure. Field-emission scanning electron microscopy (FESEM) analysis revealed their spherical shape with a diameter of about 16 nm. Vibrating sample magnetometer (VSM) was used to record the M_s value which decreased with an increase in Co^{2+} doping with negligible M_r and H_c, showing

their superparamagnetic behavior. At a low dopant (Co^{2+}) molar concentration of 0.1, spin-spin interactions dominate and beyond 0.2, the relaxation mechanism is governed by spin-lattice interactions (Sonia et al., 2022). In a similar study by Kumar *et al.* , the stable kerosene-based cobalt-doped ferrite nanofluids, termed nano-magnetic fluids (NMFs) were prepared. The dispersed NMFs were synthesized by the wet chemical (co-precipitation) method. XRD analysis confirmed the cubic single-spinel phase. In this study, the effect of varying cobalt concentrations on the magnetic properties of NMFs was analyzed. The different concentrations of cobalt were chosen (0-0.8, with an interval of 0.2). It was found that by incorporating an optimized cobalt concentration (0.2%), the M_s value rose from 43.87 to 61.78 emu/g. This can be because of the arrangement of cations on octahedral and tetrahedral sites. At 0.2% Cobalt concentration, Co^{2+} replaces Fe^{3+} at tetrahedral sites, which improves the exchange interactions between octahedral and tetrahedral sites which is then responsible for improving the magnetic properties of NMFs. With increasing dopant (Cobalt) concentration beyond critical concentration, a decrease in M_s was observed due to the decreased exchange interactions. This indicates that the change of ionic distribution in the structure significantly influences the magnetic properties. Therefore, optimal dopant concentration helps improve the properties of NMFs (Kumar et al., 2021). It is reported that Co^{2+}replaces Fe^{2+} at B sites giving ionic distribution as $(Fe^{3+})_A[Fe^{2+}{}_{1-x}Co^{2+}{}_xFe^{3+}]_BO_4$. As Fe^{3+} is distributed uniformly among A and B sites and its magnetic dipole moment is antiferromagnetically coupled, the net magnetic moment (μ) results from the divalent cations (Fe^{2+}) on the B-site. The decrease in the Ms values is due to the fact that Co^{2+} has a lower magnetic moment of 3 μ_B as compared to both Fe^{2+} (4 μ_B) and Fe^{3+} (5 μ_B). In another study by Leonel *et al.* , superparamagnetic cobalt-doped magnetite NPs were synthesized by the co-precipitation method. Doping was carried out with 3, 5, and 10 mol % of Co in ferrite NPs. The VSM study revealed the superparamagnetic nature of the synthesized NPs. M_s values for all the samples were found to be in the range of 19-25 emu/g. Also, it was observed that with the incorporation of Co, magnetocrystalline anisotropy increased by the replacement of Fe^{2+} with Co^{2+}. An increase in the coercivity was observed for the doped samples which is associated with the high anisotropic systems. The dose-dependent cytotoxic response was observed for pristine IONPs and Co-doped IONPs. MNPs doped with 10 mol% Co induced higher cytotoxicity towards cancerous cells. Upon testing on HEK 293T (normal cells) and U87 (cancer cells), their EC50 was found to be ˜24 and 17 µg/mL, respectively in the case of pristine IONPs which then reduced to ˜10 and 9 µg/mL, respectively upon incubation with 10 mol% Co-doped IONPs. This study showed that small-sized ferrite NPs (7-8 nm) hyperthermia performance can be improved by cobalt doping (Leonel et al., 2021).

Magnetic nanoparticles have been considered widely for various biomedical applications, cancer treatment being one of them. Thus, extensive research is being carried out to enhance their biocompatibility. Garanina *et al.* made an attempt to study the biocompatibility of cobalt-doped ferrite NPs *in-vivo* . Citrate functionalized 12 nm cobalt doped ferrite NPs were synthesized. The effect of different doses of MNPs on both the sexes of mice and rats for 30 days was investigated. As can be seen from Figure 9a, a dramatic weight loss was observed in the case of male mice after the injection of the maximum dosage of $CoFe_2O_4$ NPs (3000 mg/Kg) on the 14^{th} day. While in the other experimental group of mice (both male and female), no significant difference was observed in their body weights as compared to the intact group of animals over the entire incubation period (Figure 9a, 9b). Also, as seen in Figures 9c and 9d, in the case of male and female rats no statistically significant difference in their body weights was observed for all the concentrations of injected MNPs. The investigation of animal's weight, blood biochemical and animal behavioral changes revealed that as-prepared MNPs do not have the severe toxic effects at concentrations considered safe for use in clinical applications. Gender-based studies showed that male animals were affected more by MNPs dosage than female animals. This could be because of the differences in the immune responses of male and female animals. Female animals (mice and rat) showed higher phagocytic activity. Moreover, these NPs showed a high SLP value of 400 W/g. After intertumoral injection, MNPs retained the magnetic properties for several hyperthermia cycles for three days (Garanina et al., 2021).

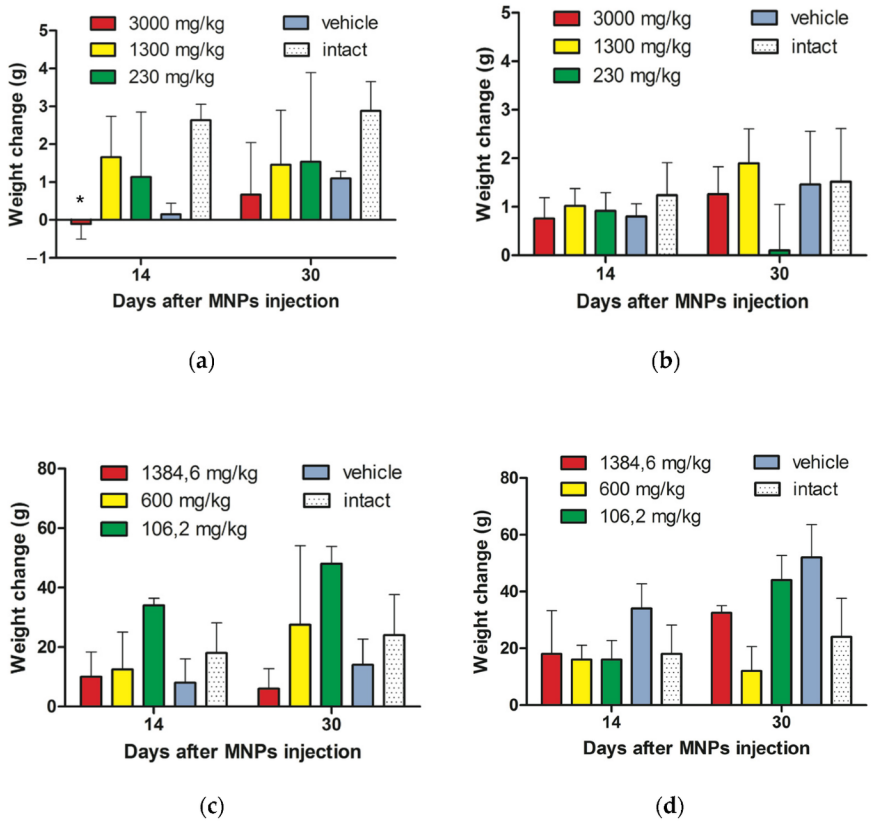

Figure 9: Animals body weight changes after $CoFe_2O_4$ NPs injection as compared to the intact animals group: (a) in case of male mice for five different experimental groups, (b) in case of female mice, (c) in case of male rats, (d) in case of female rats. Adapted from ref. (Garanina et al., 2021).

Further, in a study by Andhare *et al.* , the effect of increasing Zn concentrations on the structural, optical and magnetic properties of the Cobalt-ferrite NPs was analyzed. Zn doped cobalt Co-ferrites were prepared via a coprecipitation synthesis route. XRD revealed their cubic-spinel single-phase structure. Scanning electron microscopy (SEM) images showed the spherical grain-like structures and a decrease in agglomeration with increasing Zn concentration. Also, the saturation magnetization was found to decrease from 60.63 emu/g for Co-ferrite NPs to 43.57 emu/g for Zn doped Co-ferrites NPs (at a maximum concentration of Zn) (Andhare et al., 2020). This may be attributed to the non-magnetic nature of Zn or due to the decreased exchange interactions. Unlike, zinc ferrites, cobalt ferrites are hard magnets. Also, Zn^{2+} having zero magnetic moments replaces Fe^{3+} at the A-site which decreases the magnetic moment at the tetrahedral site. At B-site, the presence of Fe^{3+} and Co^{2+} enhances the B-B exchange-interactions with the weakening of the A-B interactions. This leads to a decrease in the magnetic properties of cobalt-ferrites.

Manohar *et al.* investigated the effect of Nickle substitution on structural and magnetic properties of Mg-ferrites ($MgFe_2O_4$). Their photocatalytic activity and cytotoxicity studies were also carried out. The solvothermal technique was employed to prepare the cubic spinel nanoferrites in 8-10 nm size range. M_s values for the as-prepared NPs were found to lie between 40.7-48.2 emu/g with a specific heat generation rate lying between 97-328 W/g. The cytotoxicity analysis of the functionalized-NPs was done on MCF-7 and MDA-MB-231 (breast cancer cells) and keratinocytes (normal cells). The functionalized-NPs were found to be biocompatible with the normal cells but were able to reduce cancer cell viability to 23-60% at concentrations of 25-1000 $\mu g\ mL^{-1}$ via ROS generation and ferroptosis (Manohar, Vijayakanth, et al., 2021). Ni doped Zn ferrites are exploited as self-controlled heaters because of their moderate M_s and low coercivity. Anu et

al. synthesized the Zn-doped Nickle (Ni) ferrite NPs via a co-precipitation process. The structural analysis revealed their cubic-spinel, face-centered structure. The maximum M_s value of 30 emu/g was obtained for NPs doped with a critical dopant concentration of 0.2, beyond which it was found to decrease. This is because of the variation in exchange–interactions as the bond angle between divalent cations and oxygen reaches 180° beyond the critical dopant concentration (0.2 molar) (Anu & Hemalatha, 2022).

Doped IONPs, particularly rare earth-doped (RE-doped) nanoferrites have proven to show improved performance as compared to pure iron oxide. For that reason, RE doped nanoferrites are suitable for hyperthermia applications (Martinez-Boubeta et al., 2013). RE-doped Fe_3O_4 shows higher magnetic-moments and a relatively larger diameter (S. S. Laha et al., 2022). Also, it shows stronger spin-orbit-coupling which is responsible for causing strain in Fe_3O_4 lattice thereby, enhancing the anisotropy and magnetization. RE-doping induced enhancement in M_s value of Fe_3O_4improves the performance of nanoferrites in hyperthermia (Niculaes et al., 2017). In a study by Fopase *et al.* , the effect of doping yttrium (RE-metal) on IONPs was analyzed. This study aimed at realizing the potential of yttrium doped IONPs for magnetic hyperthermia applications. The chemical synthesis approach, sol-gel method was utilized to obtain the desired nanoparticles. The dopant concentration was chosen to be 0.25, 0.5, 0.75 and 1 M. TEM analysis revealed agglomerated particles with an average particle size of 121 ± 57 nm. VSM studies showed the highest value of saturation magnetization of 22.68 emu/g for 0.5 M yttrium doped IONPs calcinated at 1000 °C. The induction heating studies showed 0.5 M yttrium doped IONPs possessing a SAR value of 114.65 W/g, reached hyperthermia temperature of 42-44 °C in nearly 13 min. The prepared samples were found to be biocompatible with ¿90 % cell viability when tested against MG63 cells. On the other hand, cancer cell viability was reduced to 55 % after hyperthermia treatment for 15 min. This study concluded the potential of yttrium doped IONPs as magnetic hyperthermia candidates for cancer treatment (Fopase et al., 2020). In a similar study by Kowalik *et al.* , different concentrations (0, 0.1, 1, 10 %) of yttrium were doped into Fe_3O_4 NPs to realize their hyperthermic potential. M_s value was found to be the highest with 1% dopant concentration after which the M_s value kept on decreasing. This can be ascribed to the lattice chemistry where Y^{3+} in smaller amounts stabilizes Fe^{3+} at octahedral sites. 0.1% Y^{3+}doped sample showed the best hyperthermic performance with a SAR value of 194 W/g. The prepared samples were found to be biocompatible with excellent cell viability. On the other hand, 4T1 cancer cell viability was found to reduce by 72% upon incubation with 0.1 mg/mL of 0.1% Y^{3+} doped sample under AMF. This study indicated the applicability of Y^{3+} doped Fe_3O_4 for MHT (Kowalik et al., 2020).

Besides improving the magnetic properties of MNPs for hyperthermia performance, RE metals can also impart antibacterial properties to the MNPs. In a study, Elayakumar *et al.* prepared Cerium doped cobalt-ferrite NPs by sol-gel technique. The effect of Cerium (Ce^{3+}) doping on structural, magnetic, antibacterial properties and morphology were studied. XRD and EDX (Energy Dispersive X-ray) revealed the cubic-spinel nature and single/pure phase formation of Ce^{3+} doped Co-ferrites. TEM (Transmission electron microscopy) analysis revealed sharp-edged random shaped NPs with facetted morphology. With increasing Ce^{3+}concentration, the M_s value and grain size were found to decrease whereas, the antibacterial activity of the NPs was found to increase. The maximum Ce^{3+} concentration (x = 0.5) was found to be more effective against *Klebsiellapneumoniae*(gram-positive bacterium) than *Staphylococcus aureus*(gram-positive bacterium) (Elayakumar et al., 2019). In another study by Velho-Pereira *et al.* , the antibacterial potential of Cobalt-ferrite NPs doped with Bi^{3+}, Nd^{3+} and Gd^{3+} metal ions against MDR (multidrug-resistant) bacteria was evaluated. Sol-gel combustion method was employed to obtain mono-phasic poly-crystalline NPs. TEM images revealed the particles agglomerated nature with an average diameter of 40 nm. With the increase in doping, a decrease in the size of particles was seen. Further doping of Co-ferrites increased their bactericidal efficiency against *E. coli* as compared to pristine NPs and to other metal-oxide (aluminum oxide, magnesium oxide, zirconium oxide, etc.) doped ferrites. Doping with Bi^{3+} increased the bactericidal efficiency by two folds as compared to pristine NPs against*S. epidermidis* . This study showed that doping improved the antibacterial activity of ferrite NPs, except for Gd-doped ferrites in the case of *E. coli* (Velho-Pereira et al., 2015). The various iron-based nanomaterials used for hyperthermia applications are listed in Table 3 below.

Table 3: Iron-based nanomaterials used for magnetic hyperthermia applications

Nanomaterial	Synthesis Method	Modifiers	Variant (x = mol %)	Size (nm) & shape	Magnetic Properties	Magnetic Properties	Magnetic Properties	Conc (mg/ml)	Hyperthermia Properties	Hyperthermia Properties	Hyperthermia Properties	T_H ()	Time (min
					M_S (emu/g)	H_C (Oe)	M_R (emu/g)		f (kHz)	I (kA/m)	SAR (W/g)		
Fe_3O_4	Co-precipitation	NA	NA	19 ± 3 Cubic	95	250	-	4	520	29	2453 W/g	43	60
$Co_x.Fe_{3-x}O_4$	Co-precipitation	Oleic acid	0	16, Spherical	3.18	3.056	0.008	NA	NA	NA	NA	NA	NA
			0.1		3.07	1.318	0.003						
			0.2		3.09	2.536	0.008						
			0.3		2.45	8.341	0.009						
$Co_x.Fe_{3-x}O_4$	Wet chemical co-precipitation	Oleic acid	0	15-20, Spherical	43.87	69.84	3.01	NA	NA	NA	NA	NA	NA
			0.2		61.78	31.45	2.29						
			0.4		56.78	128.14	5.83						
			0.6		42.55	128.36	4.31						
			0.8		26.18	91.77	2.01						
$Co_x.Fe_{3-x}O_4$	Co-precipitation	Carboxy-methyl-cellulose	0	7-8, Spherical	19-25	NA	NA	0.15	112.6	19.9	7.5	NA	30
			3								11.8		
			5								13.3		
			10								13.8		
$Co_x.Fe_{1-x}O_4$	Co-precipitation	Citrate	NA	12	65.3	NA	NA	0.25	375	NA	400	46-48	30
$Co_{1-x}.Zn_X.Fe_2O_4$	Co-precipitation	NA	0	NA, Spherical	60.63	3309	43.52	NA	NA	NA	NA	NA	NA
			0.3		56.66	2680	41.03						
			0.5		50.14	2226	33.39						
			0.7		48.84	1639	32.11						
			1		43.75	1630	29.24						
$Zn_xNi_{1-x}Fe_2O_4$	Co-precipitation	NA	0	16-30, Spherical	30	˜ 0	˜0	NA	NA	NA	NA	NA	NA
			0.1										
			0.2										
			0.3										
			0.4										

Nanomaterial	Synthesis Method	Modifiers	Variant (x = mol %)	Size (nm) & shape	Magnetic Properties	Magnetic Properties	Magnetic Properties	Conc (mg/mL)	Hyperthermia Properties	Hyperthermia Properties	Hyperthermia Properties	T_H ()	Time (min
$Mg_{1-x}Ni_xFe_2O_4$	Solvothermal	NA	0.1	8-10 Spherical	40.72	NA	NA	0.25-1	316	35.28	97-328	>43	8
			0.2		42.35								
			0.3		44.75								
			0.4		46.09								
			0.5		48.78								
$NiFe_2O_4$	Thermal decomposition	Oleic acid and tetramethylammonium hydroxide	NA	4.4	40.8	NA	NA	4.5	170	23.7	11	45	10
$Y_3Fe_5O_{12}$	Sol-gel	NA	0.5	121	22.7	48.5	2.3	1	336	12.9	114.6	44	13

Surface functionalization and approaches to achieve site-specificity

Surface functionalization/surface coating can be carried out in order to make these nanomaterials colloidally stable, biocompatible and site-directed. It can be performed through physical, chemical or biological routes, as shown in Figure 10. Physical modification is achieved mainly through adsorption i.e., van der Waals interactions. Chemical modification involves covalent and other strong intermolecular interactions. In case of biological modifications, a biomacromolecule is attached to the surface either via physical or chemical routes.

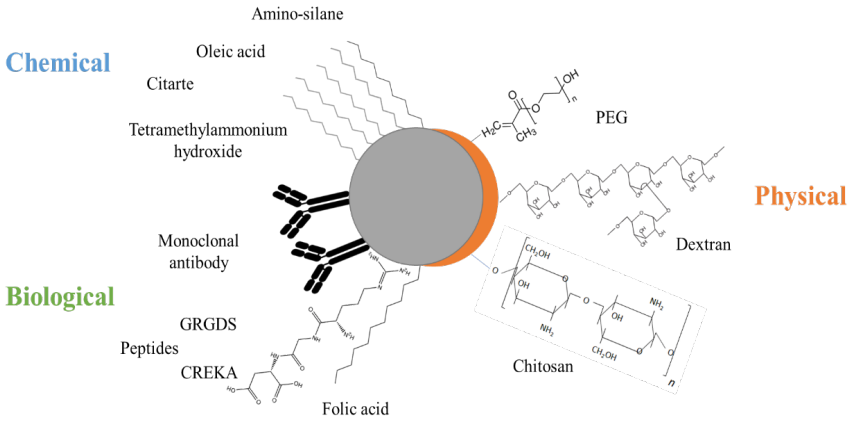

Figure 10: Different approaches and various moieties employed for surface modification of NPs

Physical modification

Various organic/inorganic polymers, biopolymers and surfactants, such as polyethylenegylcol (PEG), polyvinyl alcohol (PVA), dextran, chitosan, polyvinyl pyrrolidone (PVP), oleic acid and hyaluronic acid (HA), have been explored to carry out physical coating/functionalization (S. S. Laha et al., 2022). Various polymers used and the polymer type (end-grafted, surface adsorbed, phospholipids and di-block or co-polymers) are shown in Figure 11. Surface modification also enhances the blood-circulation time which prolongs the duration for nanomaterials to be immuno-recognized and cleared by macrophages. PEG modification not only improves the colloidal dispersion, biocompatibility and stability but also increases the blood-circulation time of MNPs by minimizing non-specific interactions. Similarly, dextran is known for its antithrombotic property. It is water-soluble, biocompatible, has high bio affinity and has a longer blood circulation time. It is one of the most utilized coatings (Strbak et al., 2020). Thus, the smaller size of MNPs and enhanced blood-circulation time improve their tissue permeability and retention, called the Enhanced Permeability and Retention (EPR) effect. However, surface functionalization/coating leads to a decrease in M_s value due to the non-magnetic nature of coated molecules. For example, PEGylated-Fe_3O_4 NPs exhibited a decrease in M_s value to 34 emu/g, as compared to bare nanoparticles with M_s value of 65-70 emu/g (Suvra S Laha et al., 2017; Xiao et al., 2014). Interestingly, in another study by Andhare *et al.* , SAR value was found to increase after PEG coating. The morphological, structural and magnetic properties of uncoated and PEG coated Zn doped Co-ferrites were studied. The SAR values of samples with concentrations of 2-8 mg/mL were found to lie in the range of 135-167 W/g and 141-217 W/g for the uncoated NPs and PEG coated, respectively. This could be because of the lower agglomeration due to the coating of NPs (Andhare et al., 2022).

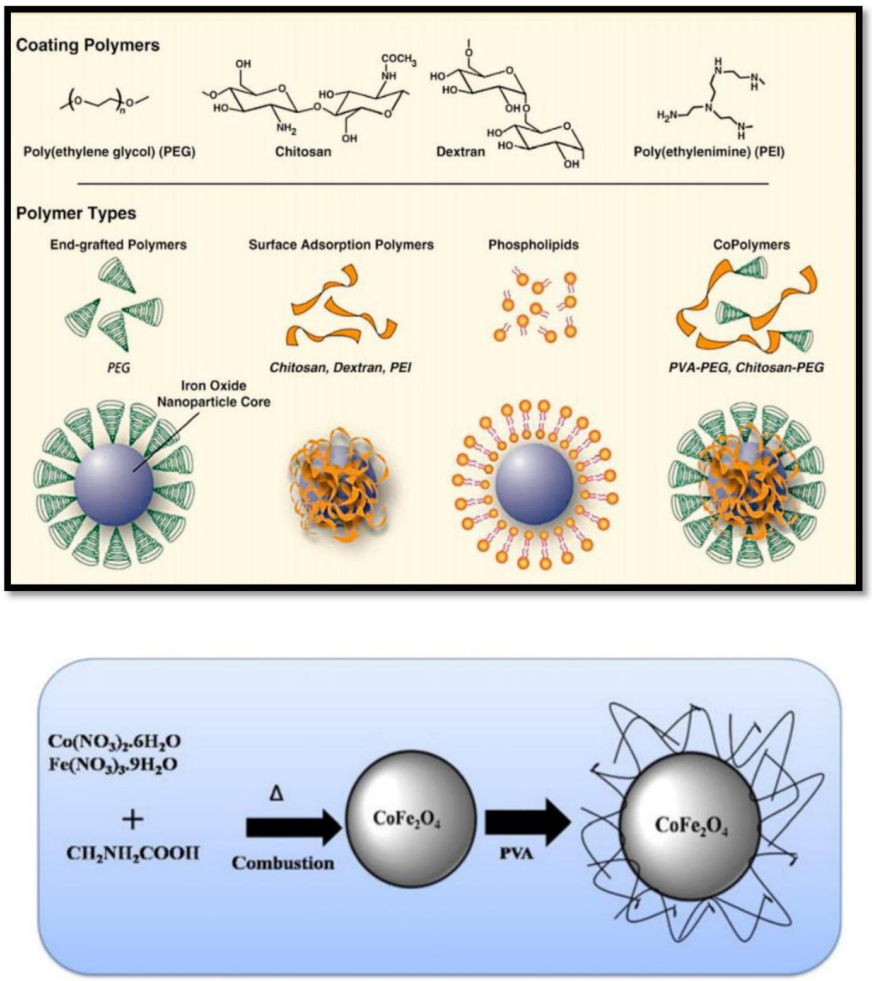

Figure 11: Various polymers used for surface coating of MNPs. The type of polymers are also depicted as end-grafted, surface adsorbed, phospholipids and co-polymers. Adapted with permission from ref. (Veiseh et al., 2010).

Quinto *et al.* synthesized PEG-coated SPIONs to study the effect of polymeric coating on their heating ability. Thermal decomposition method was used to synthesize monodispersed SPIONs bearing core diameter of 14 nm, with the use of oleic acid oleylamine as a surfactant to stabilize the NPs. Furthermore, the prepared NPs were loaded with DOX for realizing the potential of thermo-chemotherapy towards cancer treatment. To ensure their solubility, SPIONs were coated with DSPE-PEG. Two different molecular weights DSPE-PEG were used, namely 2000 and 5000 kDa. The lipid chain of phospholipid-polymer was conjugated to carbon chains of oleic acid. The SAR values for the PEG-lengths were not found significantly different, i.e., 371 and 425 W/g for PEG-2000 and PEG-5000, respectively. DOX was loaded to SPIONs with a mass ratio of 1:1. DOX release from SPIONs coated with PEG-2000 was found higher than from that of 5000. The slower drug release rate from PEG-5000 can be attributed to the presence of long PEG chains. An attempt was made to estimate the internalized iron concentration, which was found to be 455 μg/mL and is sufficient for MFH. On subjecting HeLa cells to free DOX followed by MHT, a higher additive effect was observed in terms of cytotoxicity as compared to DOX-loaded SPIONs and to individual treatments. This observation could be ascribed to the slow release of drugs from PEG-coated SPIONs but the fact cannot be neglected that polymer coating masks the NPs from macrophage recognition and also allows for targeted delivery. This study suggested that the DOX-loaded PEG-coated SPIONs can efficiently deliver a drug to cancer cells and

sufficient SPIONs internalization is capable of achieving hyperthermia temperature (Quinto et al., 2015).

Jamir *et al.* studied the effect of the surface coating of chitosan and dextran on ferrite NPs. The magnetite NPs were prepared from solvo-thermal synthesis. The ratio of biopolymer to NPs was 0.5. HRTEM analysis confirmed the spherical morphology of samples. The average size of uncoated NPs was 550 nm which was reduced to 392 nm and 388 nm for chitosan-coated and dextran-coated NPs, respectively. The biocompatible coating of chitosan and dextran reduces the aggregation of NPs, which in turn enhances the Brownian motion. $M_s$value was found to decrease from 71.05 emu/g for uncoated NPs to 69.83 emu/g for chitosan-coated and 68.23 emu/g for dextran-coated NPs which could be attributed to the presence of non-magnetic moieties on the surface of NPs. But the surface functionalization of NPs with dextran was found to enhance the SAR value by 40% i.e., 144.08 (uncoated) to 233.28 Wg^{-1} (dextran-coated) and 161.15 for Wg^{-1} (chitosan-coated) due to reduction in dipole-dipole interactions after the surface modification. The modified NPs resulted in more than 90% cell viability, proving their potential for hyperthermia applications (Jamir et al., 2021).

Nahar *et al.* investigated the role of chitosan coating on Folate-conjugated Co-ferrites (FCCF). M_s value was found to decrease from 64.4 to 55.4 emu/g after chitosan coating. High SLP values were observed even for less concentrated samples (0.5-2 mg/mL). The less concentrated samples were found to be biocompatible but at higher concentrations of 4-6 mg/mL a noticeable decline in HeLa cell viability was observed. The study suggested FCCF NPs at low concentrations could attain hyperthermia temperature and are also biocompatible (Nahar et al., 2022).

Zhila *et al.* fabricated biocompatible dextran-coated Fe_3O_4 NPs via a co-precipitation process. In this study, the ratio of dextran to NPs varied from 1:1 and 2:1. A decrease in the M_s value after dextran coating was observed, which may be attributed to the presence of non-magnetic dextran coating on MNPs. Bare NPs had M_s value of 58.91 emu/g which was reduced to 27.49 and 25.12 emu/g in case of 1:1 and 2:1 ratios, respectively. Thermogravimetric analysis (TGA) showed that 60% weight of the as-prepared NPs consisted of dextran shell. Further, the size reduction was seen with the coating. The average diameter of bare NPs was 17.8 nm, which was reduced to 14 and 10.7 nm after coating with 1:1 and 2:1 ratios, respectively. The role of dextran was attributed as a surfactant, which inhibited the further nucleation of NPs after being encapsulated. The higher ratio of dextran was found to improve biocompatibility (Shaterabadi et al., 2017).

Chemical modification

Surface functionalization can be carried out chemically via covalent conjugation and noncovalent binding. Ligand-receptor affinity can be exploited to perform the non-covalent binding. Besides electrostatic interaction and π-π bond, cargo encapsulated in phospholipid vesicles and polymers are also used for non-covalent binding. Reactive ligands make it possible to conjugate them directly to the surface of NPs via covalent conjugation. Approaches like chemisorption on NPs surface through thiol-derivatives, silane-coupling agents, adapter molecules and dative binding fall under the covalent conjugation strategy (Thiruppathi et al., 2017). Silanization using amino-silane is a common practice. The commercialized hyperthermia agent, NanoTherm® also employs amino-silane for surface modification (*magForce*). Maier-Hauff *et al.* used commercially available aminosilanized-nanofluid from MagForce to conduct clinical trials on 14 patients having glioblastoma multiform (GBM). GBM is one of the lethal forms of cancer. Localized heating and targeted drug delivery make MNPs-mediated hyperthermia a promising approach for GBM treatment. In Europe, MHT has been approved for GBM. In this study, 15 nm diameter NPs at a concentration of 112 mg/mL were used in the study. The patients received thermotherapy followed by the radiation therapy session of 16-70 Gy with single fraction of 2 Gy/cycle. This deep cranial thermo-radio therapy was well tolerated by patients under observation. The study concluded the potential of aminosilanized-MNPs for treating brain tumours safely (Maier-Hauff et al., 2007).

Khan *et al.* explored chemical surface modification for thermal chemotherapy. PEG-dicarboxylic acid (PEGD) coated MNCs were prepared by a solvothermal method. Further, the prepared MNCs were chemically amidated using hydrazine and ethyl (dimethylamino propyl) carbodiimide (EDC). These amine-modified MNCs

were conjugated with doxorubicin (DOX) as shown in Figure 12. The PEGD-coated MNCs showed a negative surface charge of -32.2 mV at pH 7.0. The carboxyl groups of PEGD interacted with the amine group of hydrazine hydrate. The nanoclusters possessed an inverse-spinel structure and crystallite size of about 15.9 nm with a Ms value of 72 emu/g. The PEGD coating resulted in a high degree of dispersity in water, DMEM and PBS. The prepared MNCs at 1mg/mL of concentration reached to the hyperthermic temperature in less than 7 minutes in water, DMEM and PBS under an applied magnetic field of 27.09 kA/m. Further DOX was attached to the amine group of hydrazine through the carbonyl group for thermal chemotherapy. A high DOX encapsulation efficiency of 92 % was observed using amidated MNCs (Khan & Sahu, 2021).

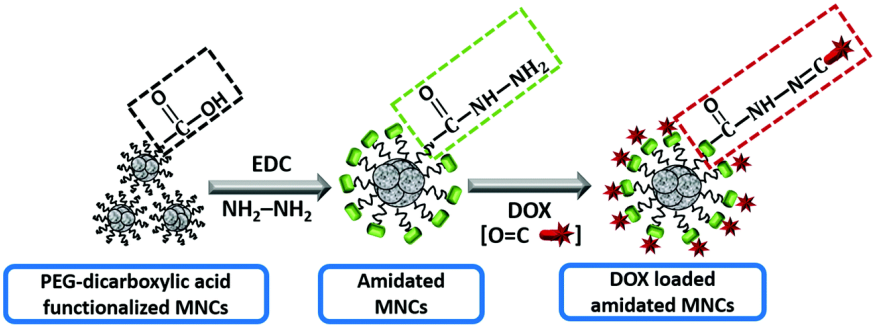

Figure 12: Schematic of surface modification of prepared NPs. EDC/NHS coupling on PEGylated MNPs surface to carry out aminosilanization and DOX conjugation to amidated surface. Adapted with permission from ref. (Khan & Sahu, 2021).

Umut *et al.* demonstrated and discussed the mechanism behind AMF-induced heating of oleic acid and tetramethylammonium hydroxide-coated nickel-ferrite NPs. Coatings were used to mask the toxic effects of Ni and to stabilize the nanoformulations. A modified co-precipitation synthesis reaction resulted in less agglomerated NPs with 4.4 nm size and ˜15 nm hydrodynamic diameter. The prepared nanoformulation exhibited superparamagnetic behavior at room temperature with a SAR value of 11 W/g within tolerable human limits of field strength and frequency i.e., H of 23.7 kAm^{-1} and f of 170 kHz. The hyperthermia temperature of about 45 °C was attained within 10 minutes leading to tumour cell necrosis. The study showed the applicability of coated $NiFe_2O_4$ for use in thermal therapy (Umut et al., 2019).

Somvanshi *et al.* studied the effect of oleic acid coating on morphological, structural, magnetic properties and colloidal stability. Magnetic hyperthermia and cytotoxicity studies were carried out to find the suitability of $MgFe_2O_4$ for biomedical applications. Interestingly, an increase in the SAR value was observed after oleic acid coating from 91 W/g for uncoated to 98 W/g for oleic acid coated NPs. This may be attributed to the colloidal stability or dispersity of NPs after oleic acid coating. Also, the coated NPs were found biocompatible even at a high concentration of 8 mg/mL (Somvanshi et al., 2020).

Biological modification

The synthesized nanomaterials can be made site-specific by conjugating biomolecules on their surfaces, such as antibodies, peptides and other ligand molecules specific to cancer cell receptors. The dispersity of NPs can be controlled by optimizing synthesis parameters and functionalization of NPs but the particle size must be less than the critical diameter to have superparamagnetic NPs possessing high magnetization. Biomolecules coating helps deliver cargo specifically to cancer cells with the least cytotoxicity (Mout et al., 2012). Besides the colloidal stability and biocompatibility, site-specificity is also highly desired for NPs to avoid their side effects on normal body cells. The site-directedness can be achieved by coating/conjugating proteins or antibodies and anti-tumour peptides (Lath et al., 2022) specific to their respective receptors which are over-expressed on cancer cells. Drug-loaded MNPs conjugated with targeting moieties commonly referred to as the targeted Drug Delivery System (DDS), which are highly desirable to achieve site-specificity.

Cancer cell targeting ligands conjugated to nanocarriers enable their specific binding to the cell surface via receptor-mediated endocytosis leading to the cellular uptake. Unlike normal cells, cancer cells over-express folate receptors. For instance, anti-HER-2-antibody, Herceptin has an avidity for HER-2 receptor which is over-expressed in breast and ovarian tumours (Jiang et al., 2008). Also, Folic-acid (FA) is a low molecular weight, stable, biocompatible/non-immunogenic and inexpensive receptor-specific ligand. There are many reports on targeting moiety (anti-Her-2-antibody, FA) conjugated, anticancer drug loaded MNPs used for combinatorial therapy (chemotherapy with hyperthermia treatment) (Choi et al., 2015; Gui et al., 2021; Mishra et al., 2020; Mu et al., 2015; Unnikrishnan et al., 2021). Yang *et al* . synthesized chitosan coated-FA fabricated-DOX loaded MNPs. DOX was loaded to MNPs with the help of a linker, tripolyphosphate (TPP). Further, to target the cancer cells specifically, FA was conjugated to DOX-loaded chitosan-coated MNPs via EDC/NHS reaction. The schematic of the modifications and DOX loading is given in Figure 13. The % drug encapsulation efficiency for DOX-MNP, Chitosan-DOX-MNP and FA-Chitosan-DOX-MNP was found to be 98.2, 91.5 and 98.6, respectively.

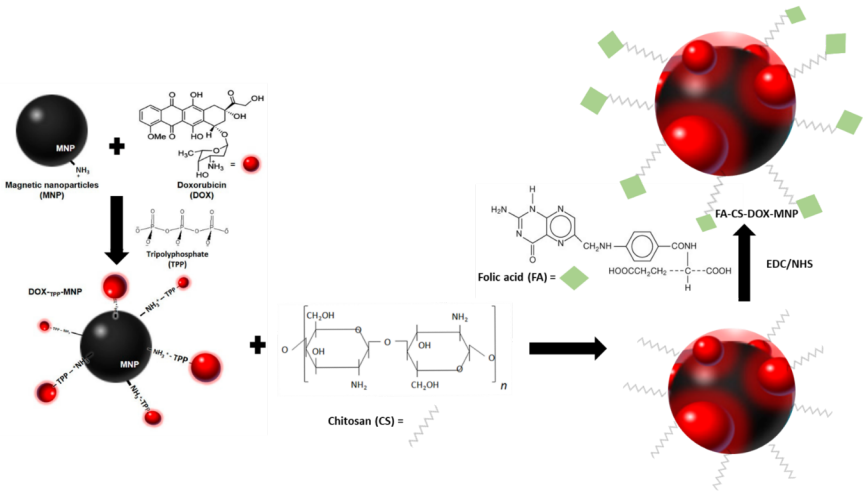

Figure 13: Schematic of DOX conjugation to MNPs via TPP linker and further grafting of FA on DOX loaded MNPs. Adapted from ref. (Yang et al., 2017)

Also, i*n-vivo* investigations of tumour volume and mouse body weight were carried out, as shown in Figure 14. Mice bearing U87 tumour were injected with FA-Chitosan-MNP, FA-Chitosan-DOX-MNP, free DOX or PBS and exposed to AMF for an hour. FA-Chitosan-DOX-MNP and free DOX were found to suppress tumour growth. Also, FA-Chitosan-DOX-MNP showed DOX delivery to tumour site and no significant body weight loss was observed. However, in the case of free DOX intravenous administration weight loss was observed. The study concluded that the FA grafted-Chitosan coated-DOX loaded-MNPs were reported to possess significantly higher toxicity towards tumour cells than MNPs without FA-grating and only DOX loaded NPs (Yang et al., 2017).

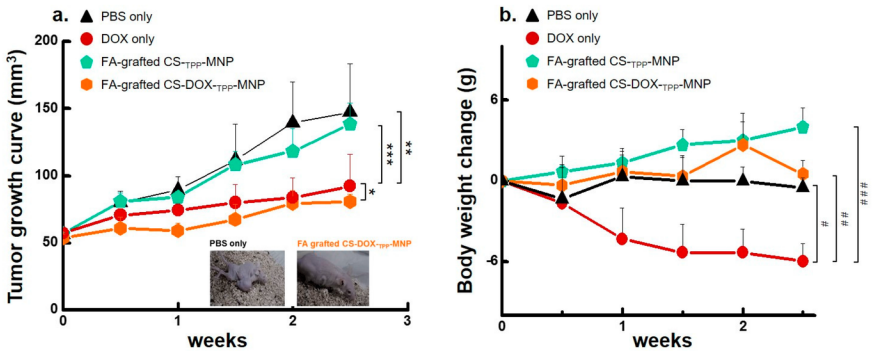

Figure 14: *In-vivo* investigations of tumour growth and mice body weight change are shown. (a) FA-Chitosan-DOX-MNPs showed tumour suppression to a great extent followed by free DOX as compared to the control (PBS), (b) the dramatic weight loss was observed in the case of free DOX whereas, FA-Chitosan-DOX-MNPs did not show any body weight loss as compared to the control (PBS). Adapted from ref. (Yang et al., 2017).

Kagawa *et al.* came up with a study based on immunotherapy combined with hyperthermia treatment to prove a novel concept of immuno-hyperthermia. They synthesized carboxydextran coated SPIONs conjugated to anti-HER2 antibody (trastuzumab) to target HER2 over-expressing breast cancer cells (AU565, SKOV-3 and NUGC-4). The conjugation of antibody to SPIONs was carried out through EDC/NHS reaction via amide linkage between –COOH group of carboxydextran coated SPIONs and $–NH_2$ of the antibody. It was observed that the antibody conjugated SPIONs were internalized within 12 hours of administration. On the other hand, unconjugated SPIONs could not target the HER-2 positive breast cancer cells. Also, conjugated SPIONs were found to be biocompatible (Kagawa et al., 2021).

Besides FA and monoclonal antibodies, tumour specific peptides such as Cys-Arg-Glu-Lys-Ala (CREKA) and arginine-glycine-aspartate (RGD) are also being used to fabricate NP-surface to achieve site-specificity. RGD peptide showed a very high affinity for binding to integrin ($\alpha_V\beta_3$ and $\alpha_V\beta_5$) (Arriortua et al., 2016), which is over-expressed on tumour cells including GBM. Senturk *et al* . synthesized ligand fabricated curcumin-loaded MNPs for GBM treatment. A peptide, glycine-arginine-glycine-aspartic acid-serine (GRGDS), was used to target GBM cells as it shows an affinity for $\alpha_v\beta_3/\alpha_v\beta_5$ domain of integrins which are over-expressed on GBM tumour cells. Curcumin is a known natural anticancer drug. It is lipophilic and can cross blood-brain barrier (BBB). Because of its poor water solubility, PLGA and PEG di-block-co-polymer was used to encapsulate curcumin-loaded SPIONs. From the mentioned ligand (GRGDS) targeted approach, It was found that the drug (curcumin) dosage was reduced to 2.5-folds as compared to the free drug and 6-folds as compared to ligand free drug loaded SPIONs. These nanocarriers could target tumour cells wherein they released about 70% of their loaded curcumin in a controlled manner and reached hyperthermia temperature within ˜15 min. The prepared multifunctional nanocarriers showed improved heating efficiency under AFM with simultaneous therapeutic efficiency against T98G cells (Senturk et al., 2021).

In another study, Du *et al.* developed a multi-modal nanoplatform capable of tumour targeting, magnetic hyperthermia therapy and MRI/MPI imaging-agent. Based on the anisotropy and crystallite size, they found that SPIONs with 18 nm size (TEM observation) can be used as efficient nanomaterials for better performance *in-vitro* , as MRI/MPI contrast agents. Their hydrodynamic size was found to be 33.1 nm with a M_s value of 60.4 emu/g. Fibrin-fibronectin complex is over-expressed in breast tumours. This complex is found to interact with its ligand CREKA. So, for achieving site-specificity, CREKA, as a tumour-targeting peptide was conjugated to the NPs via EDC/NHS coupling. They reported the zeta potential of bare NPs to be -10.34 mV which then reduced to -4.68 mV and thus confirmed the CREKA conjugation to NPs. They observed a dramatic inhibition of tumour cells without recurrence. A superior contrast was observed for MRI and MPI signals as compared to the commercially available Vivotrax. Their findings provided

researchers with a general strategy to develop multi-modal; site-directed, MRI/MPI image-guided magnetic nanoplatforms for magnetic hyperthermia and for other nanobiotechnological applications (Du et al., 2019). The biologically modified nanomaterials used for hyperthermia and/or combinatorial therapy are listed in Table 4 below.

Table 4: Biologically modified site-targeted IONPs used for hyperthermia and/or combinatorial therapy

Cancer cell type	**Receptor targeted**	**Nanoformulation**	**Modifiers**	**Synthesis route**	**Size (nm)**	**Ms (emu/g) or SAR (W/g)**	**TH () & time taken (min)**	**ὃνς. (μγ/μλ)**	**Combinatorial therapy**	**Ligand conjugated**	**Imaging modality**	**R**
Glioblastoma (T98G cells)	Integrin ($\alpha_v\beta_3/\alpha_v\beta_5$)	SPIONs	Uncoated	Thermal decomposition	5.6	6; 315	45, 15	37	Chemotherapy (Curcumin)+ Hyperthermia	cRGDS	NA	(e
			PLGA-b-PEG		142	0.3; 330						
Breast cancer cells (AU565, SKOV-3 and NUGC-4)	HER-2	SPIONs	Carboxy-dextran	Commercially available	11	NA	NA, 30	100	Immunotherapy + Hyperthermia	Trastuzumab	Staining with prussian-blue	(e
Breast cancer cells	HER-2	SPIONs	NA	NA	18	60.4, NA	NA	NA	NA	CREKA	MRI/MPI contrast agent	(a 2
HeLa cells	NA	Fe3O4 core/ZnO shell NPs	NA	Hydrothermal synthesis; deposition of ZnO	10	32; 80	45, 15	1000	NA	NA	Fluorescence imaging	(e
Human Glioblastoma (U87)	Folate	SPIONs	Chitosan	Co-precipitation	240	57.5	NA	200	Chemotherapy (DOX)+ Hyperthermia	Folic acid	NA	(e 2

Conclusion and Future Prospects

The effect of heat on biological entities was known for a long time, which triggered the studies on the hyperthermic effect on tumour cells. Biomedical field has advanced with the introduction of nanotechnology. Magnetic nanoparticles mediated hyperthermia employs magnetic nano-heaters for the purpose of generating heat to ablate cancer cells. Their surface functionalization allows for site-specific targeting and payload delivery to the diseased site. Furthermore, hyperthermia treatment can be given along with other cancer treatments such as chemotherapy or radiotherapy to sensitize cancer cells towards therapeutic drugs and radiations. Their synergistic effect enhances the overall effectiveness of the treatment. The future direction

in the development of a dual-modality nanomaterial capable of heat generation and drug delivery could involve encapsulation/conjugation of a cocktail of chemotherapeutic drugs to enhance its efficacy. Such an approach would enable to overcome patients' response variabilities towards treatment and will help in pushing it from personalized to generalized. MHT being the nascent approach among the conventional and well-established cancer treatment modalities, is restricted to adjuvant treatment. Furthermore, the effect of chemical composition and shape and size of IONPs on their heating abilities or SAR value is well-known. The development of materials in regards to improving their heating output and biocompatibility would play a crucial role in taking MFH to clinical grounds. For instance, there are fewer reports on the effect of various shapes on the SAR value of Co-ferrites. Also, the *in-vivo*toxicity assessment of Ni-ferrites and their use as hyperthermia agents are less numerous. Therefore, future studies on the evaluation of doped-ferrites heating parameters as a function of various shapes and sizes and toxicity assessment will allow for the development of potential nanoplatforms for MHT. Despite having ample literature and clinical interests in this field, acceptance of hyperthermia as a clinically available cancer treatment strategy is yet to be a reality. Also, the progression of preclinical trials to clinical trials can be seen hardly. The major challenge is to deliver heat to the deep-seated tumours uniformly and to avoid the formation of hotspots, without affecting the healthy cells. Different research groups have reported different operating conditions on field parameters which possess a hurdle in preparing a standard protocol for hyperthermia treatment. Potentiation of this field in clinical settings could be achieved by overcoming the challenges, such as lack of standard protocols, tissue temperature monitoring, defining a thermal dose and quality assurance.

References

Abraham, J., & Staffurth, J. (2016). Hormonal therapy for cancer.*Medicine* , *44* (1), 30-33. https://doi.org/10.1016/j.mpmed.2015.10.014

Aggarwal, L. J. S. P. (2014). Biological effects of ionizing radiation.*4* (1), 342-348.

Andhare, D. D., Patade, S. R., Khedkar, M. V., Nawpute, A. A., & Jadhav, K. M. (2022). Intensive analysis of uncoated and surface modified Co-Zn nanoferrite as a heat generator in magnetic fluid hyperthermia applications. *Applied Physics a-Materials Science & Processing* , *128* (6), 1-12. https://doi.org/10.1007/s00339-022-05648-0

Andhare, D. D., Patade, S. R., Kounsalye, J. S., & Jadhav, K. M. (2020). Effect of Zn doping on structural, magnetic and optical properties of cobalt ferrite nanoparticles synthesized via. Co-precipitation method. *Physica B-Condensed Matter* , *583* , 412051. https://doi.org/10.1016/j.physb.2020.412051

Anu, K., & Hemalatha, J. J. C. I. (2022). Synthesis and analysis of structural, compositional, morphological, magnetic, electrical and surface charge properties of Zn-doped nickel ferrite nanoparticles.*48* (3), 3417-3425. https://doi.org/10.1016/j.ceramint.2021.10.118

Arriortua, O. K., Garaio, E., Herrero de la Parte, B., Insausti, M., Lezama, L., Plazaola, F., Garcia, J. A., Aizpurua, J. M., Sagartzazu, M., Irazola, M., Etxebarria, N., Garcia-Alonso, I., Saiz-Lopez, A., & Echevarria-Uraga, J. J. (2016). Antitumor magnetic hyperthermia induced by RGD-functionalized Fe3O4 nanoparticles, in an experimental model of colorectal liver metastases. *Beilstein J Nanotechnol* ,*7* (1), 1532-1542. https://doi.org/10.3762/bjnano.7.147

Atkinson, W. J., Brezovich, I. A., & Chakraborty, D. P. (1984). Usable frequencies in hyperthermia with thermal seeds. *IEEE Trans Biomed Eng* , *31* (1), 70-75. https://doi.org/10.1109/TBME.1984.325372

Attaluri, A., Kandala, S. K., Zhou, H., Wabler, M., DeWeese, T. L., & Ivkov, R. (2020). Magnetic nanoparticle hyperthermia for treating locally advanced unresectable and borderline resectable pancreatic cancers: the role of tumor size and eddy-current heating. *Int J Hyperthermia* , *37* (3), 108-119. https://doi.org/10.1080/02656736.2020.1798514

Banerjee, R., Katsenovich, Y., Lagos, L., McIintosh, M., Zhang, X., & Li, C. Z. (2010). Nanomedicine: Magnetic Nanoparticles and their Biomedical Applications. *Current Medicinal Chemistry* ,*17* (27), 3120-3141. https://doi.org/10.2174/092986710791959765

Barrera, G., Coïsson, M., Celegato, F., Olivetti, E. S., Martino, L., Miletto, I., Tiberto, P. J. I. J. o. E., RF, Medicine, M. i., & Biology. (2018). Magnetic and thermal characterization of core-shell Fe-Oxide@ SiO 2 nanoparticles for hyperthermia applications.*2* (4), 257-261.

Baskar, R., Dai, J., Wenlong, N., Yeo, R., & Yeoh, K. (2014). Biological response of cancer cells to radiation treatment, Front. Mol. Biosci. 1 (2014) 1–9.

Baskar, R., Lee, K. A., Yeo, R., & Yeoh, K. W. (2012). Cancer and radiation therapy: current advances and future directions. *Int J Med Sci* , *9* (3), 193-199. https://doi.org/10.7150/ijms.3635

Blackadar, C. B. (2016). Historical review of the causes of cancer. *World J Clin Oncol* , *7* (1), 54-86. https://doi.org/10.5306/wjco.v7.i1.54

Brollo, M., Orozco-Henao, J., López-Ruiz, R., Muraca, D., Dias, C., Pirota, K., Knobel, M. J. J. o. M., & Materials, M. (2016). Magnetic hyperthermia in brick-like Ag@ Fe3O4 core–shell nanoparticles.*397* , 20-27. https://doi.org/10.1016/j.jmmm.2015.08.081

Caizer, C. J. N. (2021). Computational Study Regarding CoxFe3- xO4 Ferrite Nanoparticles with Tunable Magnetic Properties in Superparamagnetic Hyperthermia for Effective Alternative Cancer Therapy.*Nanomaterials* , *11* (12), 3294. https://doi.org/10.3390/nano11123294

Campbell, R. B. (2007). Battling tumors with magnetic nanotherapeutics and hyperthermia: turning up the heat. *Nanomedicine (Lond)* ,*2* (5), 649-652. https://doi.org/10.2217/17435889.2.5.649

Choi, W. I., Lee, J. H., Kim, J. Y., Heo, S. U., Jeong, Y. Y., Kim, Y. H., & Tae, G. (2015). Targeted antitumor efficacy and imaging via multifunctional nano-carrier conjugated with anti-HER2 trastuzumab.*Nanomedicine* , *11* (2), 359-368. https://doi.org/10.1016/j.nano.2014.09.009

Coffey, J. C., Wang, J. H., Smith, M. J. F., Bouchier-Hayes, D., Cotter, T. G., & Redmond, H. P. (2003). Excisional surgery for cancer cure: therapy at a cost. *Lancet Oncology* , *4* (12), 760-768. https://doi.org/Doi 10.1016/S1470-2045(03)01282-8

Coffey, W. T., & Kalmykov, Y. P. (2012). Thermal fluctuations of magnetic nanoparticles: Fifty years after Brown. *Journal of Applied Physics* , *112* (12), 121301. https://doi.org/10.1063/1.4754272

Compagni, A., & Christofori, G. (2000). Recent advances in research on multistage tumorigenesis. *Br J Cancer* , *83* (1), 1-5. https://doi.org/10.1054/bjoc.2000.1309

Cotin, G., Perton, F., Blanco-Andujar, C., Pichon, B., Mertz, D., & Begin-Colin, S. (2019). Design of anisotropic iron-oxide-based nanoparticles for magnetic hyperthermia (*Nanomaterials for Magnetic and Optical Hyperthermia Applications* (pp. 41-60). Elsevier. https://doi.org/10.1016/B978-0-12-813928-8.00002-8

Cristina, A., & Samia, S. J. P. N. S. M. I. (2016). Structural effects on the magnetic hyperthermia properties of iron oxide NPs. *26* , 440-448. https://doi.org/10.1016/j.pnsc.2016.09.004

Curcio, A., Silva, A. K. A., Cabana, S., Espinosa, A., Baptiste, B., Menguy, N., Wilhelm, C., & Abou-Hassan, A. (2019). Iron Oxide Nanoflowers @ CuS Hybrids for Cancer Tri-Therapy: Interplay of Photothermal Therapy, Magnetic Hyperthermia and Photodynamic Therapy. *Theranostics* , *9* (5), 1288-1302. https://doi.org/10.7150/thno.30238

Dahaghin, A., Emadiyanrazavi, S., Haghpanahi, M., Salimibani, M., Bahreinizad, H., Eivazzadeh-Keihan, R., & Maleki, A. (2021). A comparative study on the effects of increase in injection sites on the magnetic nanoparticles hyperthermia. *Journal of Drug Delivery Science and Technology* , *63* , 102542. https://doi.org/10.1016/j.jddst.2021.102542

De la Presa, P., Luengo, Y., Multigner, M., Costo, R., Morales, M., Rivero, G., & Hernando, A. J. T. J. o. P. C. C. (2012). Study of heating efficiency as a function of concentration, size, and applied field in γ-Fe2O3 nanoparticles. *The Journal of Physical Chemistry* , *116* (48), 25602-25610. https://doi.org/10.1021/jp310771p

Dennis, C. L., & Ivkov, R. (2013). Physics of heat generation using magnetic nanoparticles for hyperthermia. *International Journal of Hyperthermia* , *29* (8), 715-729. https://doi.org/10.3109/02656736.2013.836758

DeVita, V. T., Jr., & Chu, E. (2008). A history of cancer chemotherapy.*Cancer Res* , *68* (21), 8643-8653. https://doi.org/10.1158/0008-5472.CAN-07-6611

Dickson, J., & Oswald, B. J. B. J. o. C. (1976). The sensitivity of a malignant cell line to hyperthermia (42 C) at low intracellular pH.*34* (3), 262-271.

Dinarello, C. A. (2007). Historical insights into cytokines.*European Journal of Immunology* , *37* (S1), S34-S45. https://doi.org/10.1002/eji.200737772

Du, Y., Liu, X., Liang, Q., Liang, X. J., & Tian, J. (2019). Optimization and Design of Magnetic Ferrite Nanoparticles with Uniform Tumor Distribution for Highly Sensitive MRI/MPI Performance and Improved Magnetic Hyperthermia Therapy. *Nano Lett* , *19* (6), 3618-3626. https://doi.org/10.1021/acs.nanolett.9b00630

Elayakumar, K., Dinesh, A., Manikandan, A., Palanivelu, M., Kavitha, G., Prakash, S., Kumar, R. T., Jaganathan, S. K., & Baykal, A. (2019). Structural, morphological, enhanced magnetic properties and antibacterial bio-medical activity of rare earth element (REE) cerium (Ce3+) doped CoFe2O4 nanoparticles. *Journal of Magnetism and Magnetic Materials* , *476* , 157-165. https://doi.org/10.1016/j.jmmm.2018.09.089

Elion, G. B., Singer, S., & Hitchings, G. H. (1954). Antagonists of nucleic acid derivatives. VIII. Synergism in combinations of biochemically related antimetabolites. *J Biol Chem* ,*208* (2), 477-488. https://www.ncbi.nlm.nih.gov/pubmed/13174557

Esfahani, K. J. O. (2020). Roudaia L. Buhlaiga N. Del Rincon SV Papneja N. Miller WH Curr. *27* , S87-S97.

Fernandes, N., Rodrigues, C. F., Moreira, A. F., & Correia, I. J. (2020). Overview of the application of inorganic nanomaterials in cancer photothermal therapy. *Biomater Sci* , *8* (11), 2990-3020. https://doi.org/10.1039/d0bm00222d

Fopase, R., Saxena, V., Seal, P., Borah, J. P., & Pandey, L. M. (2020). Yttrium iron garnet for hyperthermia applications: Synthesis, characterization and in-vitro analysis. *Mater Sci Eng C Mater Biol Appl* , *116* , 111163. https://doi.org/10.1016/j.msec.2020.111163

Garanina, A. S., Nikitin, A. A., Abakumova, T. O., Semkina, A. S., Prelovskaya, A. O., Naumenko, V. A., Erofeev, A. S., Gorelkin, P. V., Majouga, A. G., Abakumov, M. A., & Wiedwald, U. (2021). Cobalt Ferrite Nanoparticles for Tumor Therapy: Effective Heating versus Possible Toxicity. *Nanomaterials (Basel)* , *12* (1), 38. https://doi.org/10.3390/nano12010038

Gazeau, F., Levy, M., & Wilhelm, C. (2008). Optimizing magnetic nanoparticle design for nanothermotherapy. *Nanomedicine (Lond)* ,*3* (6), 831-844. https://doi.org/10.2217/17435889.3.6.831

Gilchrist, R., Medal, R., & Shorey, W. J. A. S. (1957). Selective Inductive Heating of Lymph Nodes. *RC hanselman, JC Parrot, and CB Taylor* , *146* , 596. https://doi.org/10.1097/00000658-195710000-00007

Gilligan, M. G., Knox, P. G., Searle, P. F. J. B., & Reviews, G. E. (2000). Gene therapy: Development of immunostimulatory treatments for cancer. *Biotechnology and Genetic Engineering Reviews* ,*17* (1), 497-532. https://doi.org/10.1080/02648725.2000.10648003

Giustini, A. J., Petryk, A. A., Cassim, S. M., Tate, J. A., Baker, I., & Hoopes, P. J. (2010). Magnetic Nanoparticle Hyperthermia in Cancer Treatment. *Nano Life* , *1* (1n02), 17-32. https://doi.org/10.1142/S1793984410000067

Globocan. (2020). https://gco.iarc.fr

Gonzalez-Fernandez, M. A., Torres, T. E., Andres-Verges, M., Costo, R., de la Presa, P., Serna, C. J., Morales, M. R., Marquina, C., Ibarra, M. R., & Goya, G. F. (2009). Magnetic nanoparticles for power absorption: Optimizing size, shape and magnetic properties. *Journal of Solid State Chemistry* , *182* (10), 2779-2784. https://doi.org/10.1016/j.jssc.2009.07.047

Guardia, P., Di Corato, R., Lartigue, L., Wilhelm, C., Espinosa, A., Garcia-Hernandez, M., Gazeau, F., Manna, L., & Pellegrino, T. (2012). Water-soluble iron oxide nanocubes with high values of specific absorption rate for cancer cell hyperthermia treatment. *ACS Nano* ,*6* (4), 3080-3091. https://doi.org/10.1021/nn2048137

Gubin, S. P. (2009). *Magnetic nanoparticles* . John Wiley & Sons.

Gui, G., Fan, Z., Ning, Y., Yuan, C., Zhang, B., & Xu, Q. (2021). Optimization, Characterization and in vivo Evaluation of Paclitaxel-Loaded Folate-Conjugated Superparamagnetic Iron Oxide Nanoparticles. *Int J Nanomedicine* , *16* , 2283-2295. https://doi.org/10.2147/IJN.S287434

Gupta, J., Hassan, P. A., & Barick, K. C. (2021). Core-shell Fe3O4@ZnO nanoparticles for magnetic hyperthermia and bio-imaging applications.*Aip Advances* , *11* (2), 025207. https://doi.org/10.1063/9.0000135

Haghniaz, R., Umrani, R. D., & Paknikar, K. M. (2015). Temperature-dependent and time-dependent effects of hyperthermia mediated by dextran-coated La0.7Sr0.3MnO3: in vitro studies. *Int J Nanomedicine* , *10* , 1609-1623. https://doi.org/10.2147/IJN.S78167

Hanahan, D., & Weinberg, R. J. C. V. A.(2000). The Hallmarks of Cancer.*Cell* , *100* , 157-170. https://doi.org/10.1016/s0092-8674(00)81683-9

Hergt, R., & Dutz, S. (2007). Magnetic particle hyperthermia-biophysical limitations of a visionary tumour therapy.*Journal of Magnetism and Magnetic Materials* , *311* (1), 187-192. https://doi.org/10.1016/j.jmmm.2006.10.1156

Hu, Y., & Du, A. (2009). The Core-Shell Separation of Ferromagnetic Nanoparticles with Strong Surface Anisotropy. *Journal of Nanoscience and Nanotechnology* , *9* (10), 5829-5833. https://doi.org/10.1166/jnn.2009.1225

Hynynen, K., & Lulu, B. A. (1990). Hyperthermia in cancer treatment.*Invest Radiol* , *25* (7), 824-834. https://doi.org/10.1097/00004424-199007000-00014

Issa, B., Obaidat, I. M., Albiss, B. A., & Haik, Y. (2013). Magnetic nanoparticles: surface effects and properties related to biomedicine applications. *Int J Mol Sci* , *14* (11), 21266-21305. https://doi.org/10.3390/ijms141121266

Jamir, M., Islam, R., Pandey, L. M., & Borah, J. P. (2021). Effect of surface functionalization on the heating efficiency of magnetite nanoclusters for hyperthermia application. *Journal of Alloys and Compounds* , *854* , 157248. https://doi.org/10.1016/j.jallcom.2020.157248

Jiang, W., Kim, B. Y. S., Rutka, J. T., & Chan, W. C. W. (2008). Nanoparticle-mediated cellular response is size-dependent. *Nature Nanotechnology* , *3* (3), 145-150. https://doi.org/10.1038/nnano.2008.30

Jordan, A., Wust, P., Fahling, H., John, W., Hinz, A., & Felix, R. (1993). Inductive Heating of Ferrimagnetic Particles and Magnetic Fluids - Physical Evaluation of Their Potential for Hyperthermia.*International Journal of Hyperthermia* , *9* (1), 51-68. https://doi.org/Doi 10.3109/02656739309061478

Joshi, A., Mehta, K., Shah, H., Joshi, U., Sharma, A., & Shah, M. P. (2021). Broad spectrum application of nanotechnology for wastewater treatment (*The Future of Effluent Treatment Plants* (pp. 715-738). Elsevier. https://doi.org/10.1016/B978-0-12-822956-9.00034-9

Kagawa, T., Matsumi, Y., Aono, H., Ohara, T., Tazawa, H., Shigeyasu, K., Yano, S., Takeda, S., Komatsu, Y., Hoffman, R. M., Fujiwara, T., & Kishimoto, H. (2021). Immuno-hyperthermia effected by antibody-conjugated nanoparticles selectively targets and eradicates individual cancer cells. *Cell Cycle* , *20* (13), 1221-1230. https://doi.org/10.1080/15384101.2021.1915604

Kallumadil, M., Tada, M., Nakagawa, T., Abe, M., Southern, P., Pankhurst, Q. A. J. J. o. M., & Materials, M. (2009). Suitability of commercial colloids for magnetic hyperthermia. *Journal of Magnetism and Magnetic Materials* , *321* (10), 1509-1513. https://doi.org/10.1016/j.jmmm.2009.02.075

Kareva, I., & Hahnfeldt, P. (2013). The Emerging "Hallmarks" of Metabolic Reprogramming and Immune Evasion: Distinct or Linked?*Cancer Research* , *73* (9), 2737-2742. https://doi.org/10.1158/0008-5472.Can-12-3696

Khan, A., & Sahu, N. K. J. N. J. o. C. (2021). Hydrazone conjugated and DOX loaded PEGylated-Fe 3 O 4 mesoporous magnetic nanoclusters (MNCs): hyperthermia and in vitro chemotherapy. *45* (46), 21646-21656. https://doi.org/10.1039/D1NJ03968G

Kolosnjaj-Tabi, J., Di Corato, R., Lartigue, L., Marangon, I., Guardia, P., Silva, A. K. A., Luciani, N., Clement, O., Flaud, P., Singh, J. V., Decuzzi, P., Pellegrino, T., Wilhelm, C., & Gazeau, F. (2014). Heat-Generating Iron Oxide Nanocubes: Subtle "Destructurators" of the Tumoral Microenvironment. *ACS Nano* , *8* (5), 4268-4283. https://doi.org/10.1021/nn405356r

Kowalik, P., Mikulski, J., Borodziuk, A., Duda, M., Kaminska, I., Zajdel, K., Rybusinski, J., Szczytko, J., Wojciechowski, T., Sobczak, K., Minikayev, R., Kulpa-Greszta, M., Pazik, R., Grzaczkowska, P., Fronc, K., Lapinski, M., Frontczak-Baniewicz, M., & Sikora, B. (2020). Yttrium-Doped Iron Oxide Nanoparticles for Magnetic Hyperthermia Applications. *J Phys Chem C Nanomater Interfaces* , *124* (12), 6871-6883. https://doi.org/10.1021/acs.jpcc.9b11043

Krycka, K. L., Booth, R. A., Hogg, C. R., Ijiri, Y., Borchers, J. A., Chen, W. C., Watson, S. M., Laver, M., Gentile, T. R., Dedon, L. R., Harris, S., Rhyne, J. J., & Majetich, S. A. (2010). Core-shell magnetic morphology of structurally uniform magnetite nanoparticles. *Phys Rev Lett* , *104* (20), 207203. https://doi.org/10.1103/PhysRevLett.104.207203

Kumar, P., Pathak, S., Singh, A., Kuldeep, Khanduri, H., Wang, X., Basheed, G. A., & Pant, R. P. (2021). Optimization of cobalt concentration for improved magnetic characteristics and stability of CoxFe3-xO4 mixed ferrite nanomagnetic fluids. *Materials Chemistry and Physics* , *265* , 124476. https://doi.org/10.1016/j.matchemphys.2021.124476

Laha, S. S., Abdelhamid, E., Arachchige, M. P., Kumar, A., & Dixit, A. J. J. o. t. A. C. S. (2017). Ferroic ordering and charge-spin-lattice order coupling in Gd-doped Fe3O4 nanoparticles relaxor multiferroic system. *Journal of the American Ceramic Society* , *100* (4), 1534-1541.

Laha, S. S., Regmi, R., & Lawes, G. (2013). Structural origin for low-temperature relaxation features in magnetic nanoparticles.*Journal of Physics D-Applied Physics* , *46* (32), 325004. https://doi.org/10.1088/0022-3727/46/32/325004

Laha, S. S., Thorat, N. D., Singh, G., Sathish, C. I., Yi, J., Dixit, A., & Vinu, A. (2022). Rare-Earth Doped Iron Oxide Nanostructures for Cancer Theranostics: Magnetic Hyperthermia and Magnetic Resonance Imaging. *Small* , *18* (11), e2104855. https://doi.org/10.1002/smll.202104855

Lath, A., Santal, A. R., Kaur, N., Kumari, P., Singh, N. P. J. B., & Reviews, G. E. (2022). Anti-cancer peptides: their current trends in the development of peptide-based therapy and anti-tumor drugs.*Biotechnology and Genetic Engineering Reviews* , 1-40. https://doi.org/10.1080/02648725.2022.2082157

Laurent, S., Forge, D., Port, M., Roch, A., Robic, C., Vander Elst, L., & Muller, R. N. J. C. r. (2008). Magnetic iron oxide nanoparticles: synthesis, stabilization, vectorization, physicochemical characterizations, and biological applications. *108* (6), 2064-2110. https://doi.org/doi.org/10.1021/cr068445e

Lavorato, G., Lima, E., Mansilla, M. V., Troiani, H., Zysler, R., & Winkler, E. (2018). Bifunctional CoFe2O4/ZnO Core/Shell Nanoparticles for Magnetic Fluid Hyperthermia with Controlled Optical Response.*Journal of Physical Chemistry C* , *122* (5), 3047-3057. https://doi.org/10.1021/acs.jpcc.7b11115

Lee, S., & Margolin, K. (2011). Cytokines in cancer immunotherapy.*Cancers (Basel)* , *3* (4), 3856-3893. https://doi.org/10.3390/cancers3043856

Leonel, A. G., Mansur, A. A. P., Carvalho, S. M., Outon, L. E. F., Ardisson, J. D., Krambrock, K., & Mansur, H. S. (2021). Tunable magnetothermal properties of cobalt-doped magnetite-carboxymethylcellulose ferrofluids: smart nanoplatforms for potential magnetic hyperthermia applications in cancer therapy.*Nanoscale Advances* , *3* (4), 1029-1046. https://doi.org/10.1039/d0na00820f

Leonel, A. G., Mansur, H. S., Mansur, A. A. P., Caires, A., Carvalho, S. M., Krambrock, K., Outon, L. E. F., & Ardisson, J. D. (2019). Synthesis and characterization of iron oxide nanoparticles/carboxymethyl cellulose core-shell nanohybrids for killing cancer cells in vitro. *Int J Biol Macromol* , *132* , 677-691. https://doi.org/10.1016/j.ijbiomac.2019.04.006

Li, C., Heidt, D. G., Dalerba, P., Burant, C. F., Zhang, L., Adsay, V., Wicha, M., Clarke, M. F., & Simeone, D. M. (2007). Identification of pancreatic cancer stem cells. *Cancer Res* , *67* (3), 1030-1037. https://doi.org/10.1158/0008-5472.CAN-06-2030

magForce . https://www.magforce.com/en/home/our_therapy

Mahmood, J., Shukla, H. D., Soman, S., Samanta, S., Singh, P., Kamlapurkar, S., Saeed, A., Amin, N. P., & Vujaskovic, Z. (2018). Immunotherapy, Radiotherapy, and Hyperthermia: A Combined Therapeutic Approach in Pancreatic Cancer Treatment. *Cancers (Basel)* ,*10* (12), 469. https://doi.org/10.3390/cancers10120469

Maier-Hauff, K., Rothe, R., Scholz, R., Gneveckow, U., Wust, P., Thiesen, B., Feussner, A., von Deimling, A., Waldoefner, N., Felix, R., & Jordan, A. (2007). Intracranial thermotherapy using magnetic nanoparticles combined with external beam radiotherapy: Results of a feasibility study on patients with glioblastoma multiforme.*Journal of Neuro-Oncology* , *81* (1), 53-60. https://doi.org/10.1007/s11060-006-9195-0

Maldonado-Camargo, L., Unni, M., & Rinaldi, C. (2017). Magnetic characterization of iron oxide nanoparticles for biomedical applications (*Biomedical Nanotechnology* (pp. 47-71). Springer.

Malhotra, N., Lee, J. S., Liman, R. A. D., Ruallo, J. M. S., Villaflores, O. B., Ger, T. R., & Hsiao, C. D. (2020). Potential Toxicity of Iron Oxide Magnetic Nanoparticles: A Review.*Molecules* , *25* (14), 3159. https://doi.org/10.3390/molecules25143159

Malik, S., Kishore, S., Shah, M. P., & Kumar, S. A. J. J. o. B. M. (2022). A comprehensive review on nanobiotechnology for bioremediation of heavy metals from wastewater. *Journal of Basic Microbiology* ,*62* (3-4), 361-375. https://doi.org/10.1002/jobm.202100555

Malik, S., Prasad, S., Kishore, S., Kumar, A., Upadhyay, V. J. B., & Reviews, G. E. (2021). A perspective review on impact and molecular mechanism of environmental carcinogens on human health.*Biotechnology and Genetic Engineering Reviews* , *37* (2), 178-207. https://doi.org/10.1080/02648725.2021.1991715

Mamiya, H. (2013). Recent Advances in Understanding Magnetic Nanoparticles in AC Magnetic Fields and Optimal Design for Targeted Hyperthermia. *Journal of Nanomaterials* , *2013* . https://doi.org/10.1155/2013/752973

Manohar, A., Chintagumpala, K., & Kim, K. H. (2021). Mixed Zn-Ni spinel ferrites: Structure, magnetic hyperthermia and photocatalytic properties. *Ceramics International* , *47* (5), 7052-7061. https://doi.org/10.1016/j.ceramint.2020.11.056

Manohar, A., Vijayakanth, V., Pallavolu, M. R., & Kim, K. H. (2021). Effects of Ni - substitution on structural, magnetic hyperthermia, photocatalytic and cytotoxicity study of MgFe2O4 nanoparticles.*Journal*

of Alloys and Compounds , *879* , 160515. https://doi.org/10.1016/j.jallcom.2021.160515

Martinez-Boubeta, C., Simeonidis, K., Makridis, A., Angelakeris, M., Iglesias, O., Guardia, P., Cabot, A., Yedra, L., Estrade, S., Peiro, F., Saghi, Z., Midgley, P. A., Conde-Leboran, I., Serantes, D., & Baldomir, D. (2013). Learning from nature to improve the heat generation of iron-oxide nanoparticles for magnetic hyperthermia applications.*Sci Rep* , *3* (1), 1652. https://doi.org/10.1038/srep01652

Maurizi, M., Almadori, G., Ferrandina, G., Distefano, M., Romanini, M. E., Cadoni, G., Benedetti-Panici, P., Paludetti, G., Scambia, G., & Mancuso, S. (1996). Prognostic significance of epidermal growth factor receptor in laryngeal squamous cell carcinoma. *Br J Cancer* ,*74* (8), 1253-1257. https://doi.org/10.1038/bjc.1996.525

McCarthy, E. F. (2006). The toxins of William B. Coley and the treatment of bone and soft-tissue sarcomas. *Iowa Orthop J* , *26* , 154-158. https://www.ncbi.nlm.nih.gov/pubmed/16789469

Mishra, S., Manna, K., Kayal, U., Saha, M., Chatterjee, S., Chandra, D., Hara, M., Datta, S., Bhaumik, A., & Das Saha, K. (2020). Folic acid-conjugated magnetic mesoporous silica nanoparticles loaded with quercetin: a theranostic approach for cancer management. *Rsc Advances* , *10* (39), 23148-23164. https://doi.org/10.1039/d0ra00664e

Mohapatra, J., Zeng, F., Elkins, K., Xing, M., Ghimire, M., Yoon, S., Mishra, S. R., & Liu, J. P. J. P. C. C. P. (2018a). Size-dependent magnetic and inductive heating properties of Fe 3 O 4 nanoparticles: scaling laws across the superparamagnetic size. *20* (18), 12879-12887.

Mohapatra, J., Zeng, F., Elkins, K., Xing, M., Ghimire, M., Yoon, S., Mishra, S. R., & Liu, J. P. J. P. C. C. P. (2018b). Size-dependent magnetic and inductive heating properties of Fe 3 O 4 nanoparticles: scaling laws across the superparamagnetic size. *Rsc Advances* ,*20* (18), 12879-12887. https://doi.org/10.1039/C7CP08631H

Montazerabadi, A., Beik, J., Irajirad, R., Attaran, N., Khaledi, S., Ghaznavi, H., & Shakeri-Zadeh, A. (2019). Folate-modified and curcumin-loaded dendritic magnetite nanocarriers for the targeted thermo-chemotherapy of cancer cells. *Artif Cells Nanomed Biotechnol* , *47* (1), 330-340. https://doi.org/10.1080/21691401.2018.1557670

Mout, R., Moyano, D. F., Rana, S., & Rotello, V. M. (2012). Surface functionalization of nanoparticles for nanomedicine. *Chem Soc Rev* , *41* (7), 2539-2544. https://doi.org/10.1039/c2cs15294k

Mu, Q., Kievit, F. M., Kant, R. J., Lin, G., Jeon, M., & Zhang, M. (2015). Anti-HER2/neu peptide-conjugated iron oxide nanoparticles for targeted delivery of paclitaxel to breast cancer cells.*Nanoscale* , *7* (43), 18010-18014. https://doi.org/10.1039/c5nr04867b

Müller, R., Dutz, S., Neeb, A., Cato, A., Zeisberger, M. J. J. o. M., & Materials, M. (2013). Magnetic heating effect of nanoparticles with different sizes and size distributions. *Journal of Magnetism and Magnetic Materials* , *328* , 80-85. https://doi.org/10.1016/j.jmmm.2012.09.064

Muz, B., de la Puente, P., Azab, F., & Azab, A. K. (2015). The role of hypoxia in cancer progression, angiogenesis, metastasis, and resistance to therapy. *Hypoxia (Auckl)* , *3* , 83-92. https://doi.org/10.2147/HP.S93413

Múzquiz-Ramos, E., Guerrero-Chávez, V., Macías-Martínez, B., López-Badillo, C., & García-Cerda, L. J. C. I. (2015). Synthesis and characterization of maghemite nanoparticles for hyperthermia applications. *41* (1), 397-402. https://doi.org/10.1016/j.ceramint.2014.08.083

Nahar, A., Maria, K. H., Liba, S. I., Anwaruzzaman, M., Khan, M. N. I., Islam, A., Choudhury, S., & Hoque, S. M. (2022). Surface-modified CoFe2O4 nanoparticles using Folate-Chitosan for cytotoxicity Studies, hyperthermia applications and Positive/Negative contrast of MRI.*Journal of Magnetism and Magnetic Materials* , *554* , 169282. https://doi.org/10.1016/j.jmmm.2022.169282

Nam, P. H., Phuc, N. X., Manh, D. H., Tung, D. K., Nguyen, V. Q., Nam, N. H., Son, P. K., Bach, T. N., & Phong, P. T. (2021). Physical characterization and heating efficacy of chitosan-coated cobalt ferrite

nanoparticles for hyperthermia application. *Physica E-Low-Dimensional Systems & Nanostructures* , *134* , 114862. https://doi.org/10.1016/j.physe.2021.114862

Nemati, Z., Alonso, J., Martinez, L. M., Khurshid, H., Garaio, E., Garcia, J. A., Phan, M. H., & Srikanth, H. (2016). Enhanced Magnetic Hyperthermia in Iron Oxide Nano-Octopods: Size and Anisotropy Effects. *Journal of Physical Chemistry C* , *120* (15), 8370-8379. https://doi.org/10.1021/acs.jpcc.6b01426

Niculaes, D., Lak, A., Anyfantis, G. C., Marras, S., Laslett, O., Avugadda, S. K., Cassani, M., Serantes, D., Hovorka, O., Chantrell, R., & Pellegrino, T. (2017). Asymmetric Assembling of Iron Oxide Nanocubes for Improving Magnetic Hyperthermia Performance. *ACS Nano* ,*11* (12), 12121-12133. https://doi.org/10.1021/acsnano.7b05182

Oei, A. L., Vriend, L. E. M., Crezee, J., Franken, N. A. P., & Krawczyk, P. M. (2015). Effects of hyperthermia on DNA repair pathways: one treatment to inhibit them all. *Radiation Oncology* ,*10* (1), 1-13. https://doi.org/10.1186/s13014-015-0462-0

Oh, Y., Lee, N., Kang, H. W., & Oh, J. (2016). In vitro study on apoptotic cell death by effective magnetic hyperthermia with chitosan-coated MnFe2O4. *Nanotechnology* , *27* (11), 115101. https://doi.org/10.1088/0957-4484/27/11/115101

Patsoukis, N., Bardhan, K., Chatterjee, P., Sari, D., Liu, B., Bell, L. N., Karoly, E. D., Freeman, G. J., Petkova, V., Seth, P., Li, L., & Boussiotis, V. A. (2015). PD-1 alters T-cell metabolic reprogramming by inhibiting glycolysis and promoting lipolysis and fatty acid oxidation. *Nat Commun* , *6* (1), 6692. https://doi.org/10.1038/ncomms7692

Pyrexar Medical . (2015). https://www.pyrexar.com

Quinto, C. A., Mohindra, P., Tong, S., & Bao, G. (2015). Multifunctional superparamagnetic iron oxide nanoparticles for combined chemotherapy and hyperthermia cancer treatment. *Nanoscale* ,*7* (29), 12728-12736. https://doi.org/10.1039/c5nr02718g

Rantschler, J., McMichael, R., Castillo, A., Shapiro, A., Egelhoff Jr, W., Maranville, B., Pulugurtha, D., Chen, A., & Connors, L. J. J. o. a. p. (2007). Effect of 3 d, 4 d, and 5 d transition metal doping on damping in permalloy thin films. *101* (3), 033911. https://doi.org/10.1063/1.2436471

Reyes-Ortega, F., Checa Fernandez, B. L., Delgado, A. V., & Iglesias, G. R. (2019). Hyperthermia-Triggered Doxorubicin Release from Polymer-Coated Magnetic Nanorods. *Pharmaceutics* , *11* (10), 517. https://doi.org/10.3390/pharmaceutics11100517

Rosensweig, R. E. (2002). Heating magnetic fluid with alternating magnetic field. *Journal of Magnetism and Magnetic Materials* ,*252* (1-3), 370-374. https://doi.org/10.1016/S0304-8853(02)00706-0

Saunders, P. A., Hendrycks, V. R., Lidinsky, W. A., & Woods, M. L. (2005). PD-L2:PD-1 involvement in T cell proliferation, cytokine production, and integrin-mediated adhesion. *European Journal of Immunology* , *35* (12), 3561-3569. https://doi.org/10.1002/eji.200526347

Senturk, F., Cakmak, S., Kocum, I. C., Gumusderelioglu, M., & Ozturk, G. G. (2021). GRGDS-conjugated and curcumin-loaded magnetic polymeric nanoparticles for the hyperthermia treatment of glioblastoma cells. *Colloids and Surfaces a-Physicochemical and Engineering Aspects* ,*622* , 126648. https://doi.org/10.1016/j.colsurfa.2021.126648

Sezer, N., Ari, I., Bicer, Y., & Koc, M. (2021). Superparamagnetic nanoarchitectures: Multimodal functionalities and applications. *Journal of Magnetism and Magnetic Materials* , *538* , 168300. https://doi.org/10.1016/j.jmmm.2021.168300

Shaterabadi, Z., Nabiyouni, G., & Soleymani, M. (2017). High impact of in situ dextran coating on biocompatibility, stability and magnetic properties of iron oxide nanoparticles. *Mater Sci Eng C Mater Biol Appl* , *75* , 947-956. https://doi.org/10.1016/j.msec.2017.02.143

Simeonidis, K., Martinez-Boubeta, C., Serantes, D., Ruta, S., Chubykalo-Fesenko, O., Chantrell, R., Oro-Sole, J., Balcells, L., Kamzin, A. S., Nazipov, R. A., Makridis, A., & Angelakeris, M. (2020). Controlling Magnetization Reversal and Hyperthermia Efficiency in Core-Shell Iron-Iron Oxide Magnetic Nanoparticles by Tuning the Interphase Coupling. *Acs Applied Nano Materials* , *3* (5), 4465-4476. https://doi.org/10.1021/acsanm.0c00568

Somvanshi, S. B., Patade, S. R., Andhare, D. D., Jadhav, S. A., Khedkar, M. V., Kharat, P. B., Khirade, P. P., & Jadhav, K. M. (2020). Hyperthermic evaluation of oleic acid coated nano-spinel magnesium ferrite: Enhancement via hydrophobic-to-hydrophilic surface transformation. *Journal of Alloys and Compounds* , *835* , 155422. https://doi.org/10.1016/j.jallcom.2020.155422

Sonia, L., Phanjoubam, S. J. J. o. M., & Materials, M. (2022). Structural and magnetic studies of cobalt substituted magnetite ferrofluids. *Journal of Magnetism and Magnetic Materials* ,*544* , 168675. https://doi.org/10.1016/j.jmmm.2021.168675

Strbak, O., Antal, I., Khmara, I., Koneracka, M., Kubovcikova, M., Zavisova, V., Molcan, M., Jurikova, A., Hnilicova, P., Gombos, J., Kadasova, N., & Dobrota, D. (2020). Influence of Dextran Molecular Weight on the Physical Properties of Magnetic Nanoparticles for Hyperthermia and MRI Applications. *Nanomaterials (Basel)* ,*10* (12), 2468. https://doi.org/10.3390/nano10122468

Thiesen, B., & Jordan, A. (2008). Clinical applications of magnetic nanoparticles for hyperthermia. *Int J Hyperthermia* , *24* (6), 467-474. https://doi.org/10.1080/02656730802104757

Thiruppathi, R., Mishra, S., Ganapathy, M., Padmanabhan, P., & Gulyas, B. (2017). Nanoparticle Functionalization and Its Potentials for Molecular Imaging. *Adv Sci (Weinh)* , *4* (3), 1600279. https://doi.org/10.1002/advs.201600279

Tsopoe, S. P., Borgohain, C., Fopase, R., Pandey, L. M., & Borah, J. P. (2020). A comparative investigation of normal and inverted exchange bias effect for magnetic fluid hyperthermia applications. *Sci Rep* ,*10* (1), 18666. https://doi.org/10.1038/s41598-020-75669-3

Umut, E., Coşkun, M., Pineider, F., Berti, D., Güngüneş, H. J. J. o. c., & science, i. (2019). Nickel ferrite nanoparticles for simultaneous use in magnetic resonance imaging and magnetic fluid hyperthermia.*550* , 199-209. https://doi.org/10.1016/j.jcis.2019.04.092

Unnikrishnan, B. S., Sen, A., Preethi, G. U., Joseph, M. M., Maya, S., Shiji, R., Anusree, K. S., & Sreelekha, T. T. (2021). Folic acid-appended galactoxyloglucan-capped iron oxide nanoparticles as a biocompatible nanotheranostic agent for tumor-targeted delivery of doxorubicin. *International Journal of Biological Macromolecules* ,*168* , 130-142. https://doi.org/10.1016/j.ijbiomac.2020.11.205

Veiseh, O., Gunn, J. W., & Zhang, M. (2010). Design and fabrication of magnetic nanoparticles for targeted drug delivery and imaging. *Adv Drug Deliv Rev* , *62* (3), 284-304. https://doi.org/10.1016/j.addr.2009.11.002

Velho-Pereira, S., Noronha, A., Mathias, A., Zakane, R., Naik, V., Naik, P., Salker, A. V., & Naik, S. R. (2015). Antibacterial action of doped CoFe2O4 nanocrystals on multidrug resistant bacterial strains.*Materials Science & Engineering C-Materials for Biological Applications* , *52* , 282-287. https://doi.org/10.1016/j.msec.2015.03.046

wPeng, E., Choo, E. S., Chandrasekharan, P., Yang, C. T., Ding, J., Chuang, K. H., & Xue, J. M. (2012). Synthesis of manganese ferrite/graphene oxide nanocomposites for biomedical applications.*Small* , *8* (23), 3620-3630. https://doi.org/10.1002/smll.201201427

Xiao, N., Gu, W., Wang, H., Deng, Y., Shi, X., Ye, L. J. J. o. c., & science, i. (2014). T1–T2 dual-modal MRI of brain gliomas using PEGylated Gd-doped iron oxide nanoparticles. *Journal of Colloid and Interface Science* , *417* , 159-165. https://doi.org/10.1016/j.jcis.2013.11.020

Yang, C. L., Chen, J. P., Wei, K. C., Chen, J. Y., Huang, C. W., & Liao, Z. X. (2017). Release of Doxorubicin by a Folate-Grafted, Chitosan-Coated Magnetic Nanoparticle. *Nanomaterials (Basel)* ,*7* (4), 85. https://doi.org/10.3390/nano7040085